Engineering Fracture Mechanics 242 (2021) 107487

Contents lists available at ScienceDirect

Engineering Fracture Mechanics

journal homepage: www.elsevier.com/locate/engfracmech

Fracture mechanics based fatigue life prediction for a weld toe crack under constant and variable amplitude random block loading—Modeling and uncertainty estimation

Davide Leonetti [a,*], Johan Maljaars [a,b], H.H. (Bert) Snijder [a]

[a] Department of the Built Environment, Eindhoven University of Technology, The Netherlands
[b] TNO, The Netherlands

ARTICLE INFO

Keywords:
Linear elastic fracture mechanics
Fatigue crack growth at weld
Cyclic R-curve
Mechanically short and long cracks

ABSTRACT

Propagation of weld toe cracks under cyclic loading is often predicted using fracture mechanics. In as welded condition, most of the propagation life is spent as a short crack, which is known to behave differently than a long crack. Several studies have been conducted with the aim of correlating the fatigue crack growth rate and the threshold condition of small cracks to the well known linear elastic crack driving force parameter ΔK, the stress intensity factor range. In many cases, the application of such models requires the quantification of material properties and model parameters that are difficult to obtain from tests, and therefore scarcely available. The present paper bypasses this inconvenience by making use of the square root of area, $\sqrt{area}$, parameter proposed by Murakami. Successively, a linear elastic fracture mechanics based fatigue crack growth model is formulated for physically short and long cracks under constant and variable amplitude random block loading. The uncertainty of the model parameters is quantified in a frequentist statistical framework.

1. Introduction

The resistance of welded details against fatigue failure is often evaluated through the use of fatigue resistance curves in combination with the linear damage rule proposed by Palmgren and Miner [1–3]. For welded details, a global approach to fatigue, e.g. with the nominal or geometrical stress range as load parameters, is preferred to more local approaches based on continuum mechanics. This is because the in-service behavior of such details is largely influenced by the presence, the location, and the type of initial defects that significantly reduce the crack initiation stage of the fatigue life, up to the extent that this may even not exist in as-welded details [4]. When initial defects are assumed to exist, fracture mechanics is necessary instead of continuum mechanics to study their behavior, potentially leading to high accuracy in determining both the fatigue life and the threshold condition [5–13]. Moreover, fracture mechanics models are required for implementing DTD, i.e. a design based on periodic fatigue inspections, in both deterministic and probabilistic frameworks, for example in steel bridges [14–18]. In DTD, the fracture mechanics model aims to the determination of the fatigue crack growth rate, forming the basis to estimate inspection intervals.

Despite the crack growth being erratic [19], it is often assumed that the first mode of loading is dominant and that the crack grows in a plane. The crack path is usually evaluated through either a single parameter, i.e. the crack depth a, or two parameters, i.e. the crack depth a and the crack width $2c$. A semi-elliptical shape of the crack front is assumed [20–22], see Fig. 1. This assumption is supported by experimental observation about the crack front shapes observed in metals. Cracks observed in smooth specimens

* Corresponding author.
E-mail address: d.leonetti@tue.nl (D. Leonetti).

https://doi.org/10.1016/j.engfracmech.2020.107487
Received 10 February 2020; Received in revised form 23 November 2020; Accepted 15 December 2020
Available online 24 December 2020

Nomenclature

CA	Constant Amplitude
DTD	Damage Tolerant Design
FCGR	Fatigue Crack Growth Rate
HAZ	Heat-Affected Zone
K–T	Kitagawa–Takahashi
SIF	Stress Intensity Factor
VA	Variable Amplitude

Symbols

α''	Geometry parameter for σ_{ref}
$\Delta\sigma$	Nominal stress range
$\Delta\sigma_0$	Fatigue limit
$\Delta\sigma_{\text{rms}}$	Root mean square stress range in the stress spectrum
$\Delta\sigma_{\text{d}}$	Dispersion parameter of the Rayleigh distribution
$\Delta\sigma_{\text{max}}$	Maximum stress range in the stress spectrum
$\Delta\sigma_{\text{m}}$	Location parameter of the Rayleigh distribution
$\Delta\sigma_{\text{th}}$	Threshold stress range
ΔK	SIF range
ΔK_0	Threshold SIF range for long cracks at $R = 0$
ΔK_{rms}	Root mean square SIF range of the spectrum
ΔK_{max}	Maximum SIF range of the spectrum
$\Delta K_{\text{th,eff}}$	Intrinsic (effective) component of the threshold SIF range
$\Delta K_{\text{th,op,lc}}$	Extrinsic component of the threshold SIF range for long cracks
$\Delta K_{\text{th,op}}$	Extrinsic component of the threshold SIF range
ΔK_{th}	Threshold SIF range
$\Delta K_{th,\text{lc}}$	Threshold SIF range for long cracks
$\hat{}$	Estimator
σ_{max}	Maximum stress of the stress cycle
σ_{min}	Minimum stress of the stress cycle
σ_{m}	Primary membrane stress
σ_{op}	Crack opening stress
σ_{ref}	Reference stress
σ_b	Primary bending stress
σ_j	jth coefficient of a polynomial stress distribution
σ_s	Secondary stress
σ_u	Ultimate tensile strength
σ_y	Yield stress
$\sqrt{area}$	Square root of area parameter
$\sqrt{area}_{\text{crit}}$	Critical value of the square root of area parameter
$E\left[\frac{da}{dn}\right]_{\text{VA}}$	Average fatigue crack growth rate observed under VA loading
i	Index referring to the load level in the stress spectrum
j	Index referring to the fatigue test data
a	Crack depth
A_0	Parameter of the crack closure function
a_0	Fitting parameter for El-Haddad model
A_1	Parameter of the crack closure function
A_2	Parameter of the crack closure function
A_3	Parameter of the crack closure function
$A_{0,\Omega}$	Parameter of the crack closure function under VA spectrum loading
$A_{1,\Omega}$	Parameter of the crack closure function under VA spectrum loading
a_{crit}	Crack depth associated to $\sqrt{area}_{\text{crit}}$

a_{ini}	Initial crack depth
B	Thickness of the cross-section
C	Fatigue crack growth rate coefficient
c	Semi crack width
C_1	Integration constant
C_Ω	Fatigue crack growth rate coefficient under VA spectrum loading
c_{th}	Parameter of the NASGROW model
$CoV[\ ]$	Coefficient of variation
d	Distance from the free surface of the largest microstructural barrier
da/dn	Fatigue crack growth rate
F	Crack velocity function
F_Ω	Crack velocity function under VA spectrum loading
f_j	Weight functions
F_{lc}	Crack velocity function for long cracks
$f_{\text{op},\Omega}$	Crack opening function under VA spectrum loading
f_{op}	Crack opening function
$F_{lc,\Omega}$	Crack velocity function for long cracks under VA spectrum loading
H_{b}	Brinell hardness
H_{V}	Vickers hardness
$I(\theta)$	Fisher information matrix
K	SIF
k	Calibration parameter of the cyclic resistance curve as proposed by Mc Evily
K_c	Critical value of the SIF
k_{m}	Misalignment factor for SIF
$K_{\text{p,max}}$	SIF resulting from primary stresses at the maximum applied load
$K_{\text{p,max}}$	SIF resulting from primary stresses at the minimum applied load
K_{p}	SIF resulting from primary stresses
$K_{\text{s,b}}$	SIF resulting from secondary bending stresses
$K_{\text{s,m}}$	SIF resulting from secondary membrane stresses
$K_{\text{s,sb}}$	SIF resulting from secondary self-balancing stresses
K_{s}	SIF resulting from secondary stresses
$K_{p,b}$	SIF resulting from primary bending stresses
$K_{p,m}$	SIF resulting from primary membrane stresses
k_{tb}	Stress concentration factor for SIF under bending loading
k_{tm}	Stress concentration factor for SIF under membrane loading
M	Bulging correction factor for the SIF
m	Fatigue crack growth rate exponent
m_Ω	Fatigue crack growth rate exponent under VA spectrum loading
M_{m}	Stress intensity magnification factor for membrane stresses
M_{w}	Stress intensity magnification factor
M_b	Stress intensity magnification factor for bending stresses
$M_{w,b}$	Weld toe stress intensity magnification factor for bending stresses
$M_{w,m}$	Weld toe stress intensity magnification factor for membrane stresses
N	Number of cycles to failure
n_i	Number of cycles for the ith stress range in the spectrum
$p_{\text{th},\Omega}$	Parameter of the FCGR model under VA spectrum loading
p_{th}	Parameter of the NASGROW equation
R	Load ratio: $\sigma_{\min}/\sigma_{\max}$.
T_{w}	width of the section
Y	Geometrical correction function for the SIF
Z	Weld leg
z	Distance from the free surface of the considered point along the crack front
E[ ]	Expectation operator

Pr[ ]	Probability
St.err.[ ]	Standard error

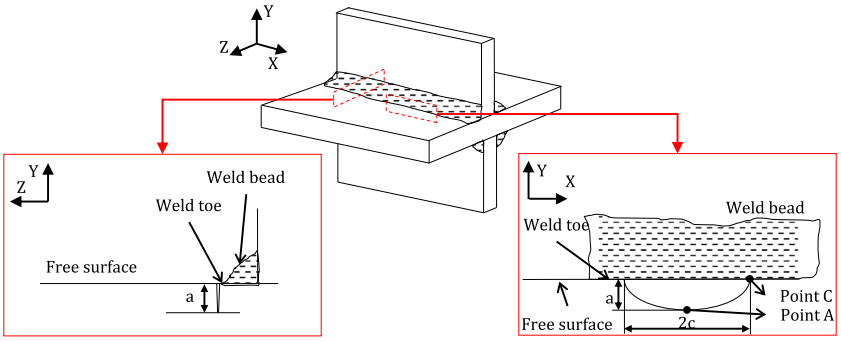

Fig. 1. Crack developing at the weld toe of a non-load-carrying cruciform joint. Strategy involving one parameter, the crack depth, a, to model the crack front, or two parameters, the crack depth, a and the semi-width, c.

are found to initiate having an aspect ratio, a/c, close to unity [23], i.e. their shape is semi-circular. Several studies involved the description of the crack growth at the weld toe in transverse welds [24–26]. These cracks are characterized by smaller aspect ratios ($a/c < 0.3$) than cracks growing at the surface of smooth specimens. Moreover, multiple initiation sites are observed along the weld toe, leading to short cracks which, especially at the early stages, tend to coalesce, forming larger cracks. When the crack depth exceeds approximately 0.3 mm, it has been found that microstructural imperfections no longer affect crack growth [24–26].

The initial crack size to be used for fatigue life prediction based on fracture mechanics has been the subject of several studies. In some of these studies, the equivalent initial flaw size is used, where the size has been determined by making use of fracture mechanics fatigue life prediction models. The equivalent initial flaw size has been determined iteratively on the basis of the agreement between the model prediction and fatigue test data [27,28]. Therefore, the initial crack size and its distribution are calibrated and are conditional to the model, limiting the application of such an initial crack size to the model used and the geometry and the load condition for which it was derived. This is because in most of these models there is no explicit reference to the distinction between short and long cracks, despite the equivalent initial crack size being often one order of magnitude smaller than one millimeter, which in the majority of the structural steels is often associated with a short crack. Zerbst [29] proposed to use as (artificial) minimum initial crack size the maximum non-propagating crack at the fatigue limit for a given load ratio R. Using the crack arrest approach Zerbst showed that the initial predicted crack size is smaller for the high-strength than for the low-strength steels [30]. On the contrary, the size of non-propagating cracks is found to decrease with increasing the strength of the steel. Following an analysis of the locations of crack initiation, no correlation was found with the geometry of the weld toe [31]. They were found to be dependent on the surface roughness and the incidence of ripples up to a certain distance from the weld toe. Moreover, in the early stages of crack propagation, the number of cracks along the weld toe was found to be proportional to the severity of the applied load, in accordance with previous literature [32]. In [33] a model is presented in which the initial crack is defined by means of a method based on a crack arrest criterion. Moreover, the initiation of multiple cracks is considered, based on the geometrical variation of the weld toe geometry. A complete description of the initial crack size is relevant for fracture mechanics-based fatigue life prediction. This can be obtained by observing fracture surfaces or by using non-destructive measurements. For example, measurements of the initial defect size are reported in [34] for Inconel weldments. However, in this case uncertainty exists about the type of weld defect or imperfection encountered since in [34] it is not stated whether the initial size reported is related to a crack, an undercut, or any other type of crack-like defect located at the weld toe.

The characterization of short and long cracks through the definition of length scales in which cracks can be defined as either “long” or “short” is not possible in absolute terms. Short cracks have been divided into microstructurally short cracks (micro-cracks), and mechanically or physically short cracks (small cracks) [35–39]. For micro-cracks, the propagation rate is significantly affected by the microstructure, and it is found to be inhomogeneous due to the effect of microstructural barriers [40], see Fig. 2. Small cracks are large enough to be not significantly affected by microstructural barriers, and they can be considered as surrounded by a homogeneous material. For this reason, the crack growth rate, da/dn, can be potentially described by means of a crack driving force parameter based on the assumption of homogeneity, as the linear elastic stress intensity factor (SIF), K. It has been extensively shown in the literature that for small cracks the measured crack growth rate plotted against the SIF range, ΔK, does not correlate well with that one of long cracks. This is because a small crack is not long enough for its driving force to be affected by extrinsic effects that typically influence the behavior of long cracks, such as plasticity, oxide and, roughness induced crack closure [37], or any other mechanism that shields the crack tip. For small cracks, the shielding effect of the crack tip is not as effective as for long cracks, because of the dimension of the crack flanks. For these reasons, early studies observe that under cyclic loading conditions leading to the same driving force, small cracks propagate faster than large cracks [23], see Fig. 2. However, the linear elastic SIF

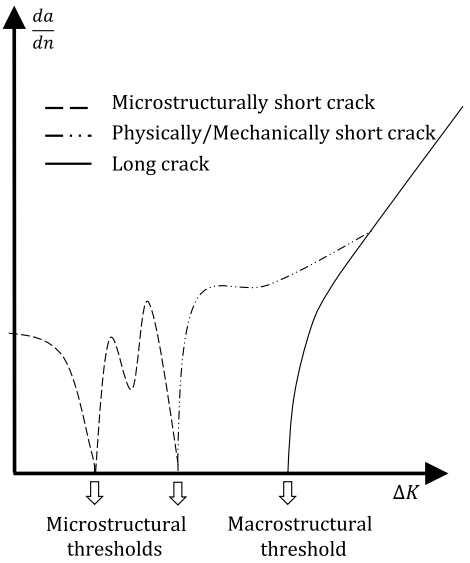

Fig. 2. Stages of fatigue crack propagation.
Source: Adapted from Miller [40].

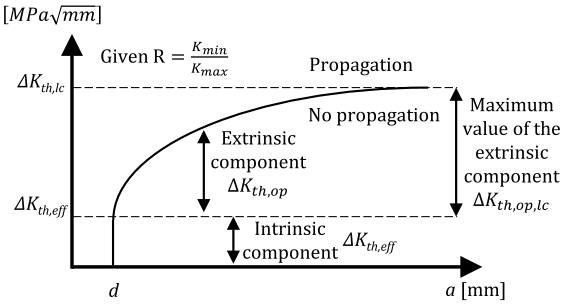

Fig. 3. Qualitative trend of the cyclic R-curve.

range, ΔK, valid only to describe the crack growth rate for long cracks, has been found suitable to describe also the growth of small cracks [41] by making explicit the dependence of the extrinsic effects and crack size. This is because the intrinsic resistance to fatigue crack propagation, which is related to the (intrinsic) damage processes that operate ahead of the crack tip [42], is essentially the same. The extrinsic effects affect the crack tip stresses. The crack tip should be open at a minimum applied stress greater than zero. When extrinsic effects occur, the above condition is not always verified and the crack opening stress σ_{op} can be greater than the minimum stress of the stress cycle, i.e. $\sigma_{op} > \sigma_{min}$, determining a reduction of the effective crack driving force.

As for the fatigue crack growth rate, a similar difference between small and long cracks is observed for the threshold condition [43]. The extrinsic mechanisms that determine a higher apparent threshold for long cracks are equal to those responsible for a lower crack propagation rate [41], despite the intrinsic mechanism of threshold phenomena and crack propagation being different [36–38]. The threshold condition, ΔK_{th}, is modeled as the sum of the intrinsic, $\Delta K_{th,eff}$, and the extrinsic, $\Delta K_{th,op}$, components, and tends to the threshold SIF range for long cracks, $\Delta K_{th,lc}$, with increasing the crack size:

$$\Delta K_{th} = \Delta K_{th,eff} + \Delta K_{th,op} \tag{1}$$

where $\Delta K_{th,op}$ depends on the crack size, a, and the load ratio, R, and its maximum value is given by $(\Delta K_{th,lc} - \Delta K_{th,eff})$. Some studies support the hypothesis that $\Delta K_{th,eff}$ depends, not only on the material, but also on the load ratio, R, despite the mechanisms causing this dependence are not clear yet [44–46]. Other studies do not make an explicit reference to this relation or support the hypothesis of the intrinsic threshold to be a unique material dependent parameter [41,47–49].

The circumstance that a small and a long crack subjected to the same ΔK exhibit different crack growth rates and require different threshold conditions is a break of the similitude principle. This implies that the modeling and the experimental data for fatigue crack propagation of small and long cracks are different. Several authors modeled the threshold condition for small cracks in different ways. By using these models, the condition for which a crack propagates under cyclic loading is $\Delta K > \Delta K_{th}$ and is graphically depicted through the cyclic resistance-curve (R-curve) [50], see Fig. 3, which related the threshold condition for crack propagation

to the crack size. Smith [51] determined the smallest crack size which is significant in linear elastic fracture mechanics calculations as dependent on the threshold SIF range for long cracks and the fatigue limit of smooth specimens. El Haddad [52] interpreted the behavior of experimental data from Kitagawa and Takahashi [43] and formulated the first model able to consider the effect of the crack size on the threshold SIF range, which is nowadays used in the NASGROW model [53] by the following equation:

$$\Delta K_{\mathrm{th}} = \Delta K_{\mathrm{th,lc}} \sqrt{\frac{a}{a + a_0}} \tag{2}$$

where a_0 is a calibration parameter called "intrinsic crack length", which according to [53] can be considered as a fixed value $a_0 = 0.0381$ mm. Zerbst [29] proposed a modified version of Eq. (2), based on the observation that ΔK_{th} should equal $\Delta K_{\mathrm{th,eff}}$ for crack extension equal to zero, that is for $a - d = 0$:

$$\Delta K_{\mathrm{th}} = \Delta K_{\mathrm{th,lc}} \sqrt{\frac{a + a^*}{a + a^* + a_0}} \tag{3}$$

where:

$$a^* = a_0 \frac{(\Delta K_{\mathrm{th,eff}} \setminus \Delta K_{\mathrm{th,lc}})^2}{1 - (\Delta K_{\mathrm{th,eff}} \setminus \Delta K_{\mathrm{th,lc}})^2} \tag{4}$$

In this approach, the intrinsic crack length is determined as:

$$a_0 = \frac{1}{\pi} \left(\frac{\Delta K_{\mathrm{th,lc}}}{Y \Delta \sigma_0} \right)^2 \tag{5}$$

where Y is the geometry correction factor, typically equal to 1 [29]. Murakami [54,55] related ΔK_{th} to the Vickers hardness, H_{V}, for several metals. The size of the defect was accounted for by the square root of the area resulting from the orthogonal projection of the defect with respect to a plane perpendicular to the loading direction, i.e. the $\sqrt{area}$ parameter. The $\sqrt{area}$ is found to be able to correlate different types of surface defects, namely notches, indentations, and cracks, with the threshold SIF range. Moreover, the correlation holds independent of the shape of the defect, see Fig. 4. The experimental data produced to relate the $\sqrt{area}$ parameter to the threshold stress for fatigue crack propagation, $\Delta \sigma_{\mathrm{th}}$, led to the definition of the critical value of the $\sqrt{area}$ parameter, $\sqrt{area}_{\mathrm{crit}}$. For defects such that $\sqrt{area} \leq \sqrt{area}_{\mathrm{crit}}$, $\Delta \sigma_{\mathrm{th}} = \Delta \sigma_0$, otherwise $\Delta \sigma_{\mathrm{th}} < \Delta \sigma_0$. To model the build-up of the extrinsic effect on the intrinsic threshold, Mc Evily [56] suggested an exponential relation of which the exponent is dependent on the material and loading condition, i.e. the load ratio. This relation was successively used by Chapetti [46] to model the cyclic R-curve by a formulation which required only one independent parameter controlling the length scale at which the extrinsic effects take place, besides the measurement of $\Delta K_{\mathrm{th,eff}}$ and $\Delta K_{\mathrm{th,lc}}$. In [41] the build-up of crack closure was modeled as the sum of two exponential terms that have to be calibrated with test data. The two terms take independently into consideration the plasticity and roughness induced crack closure and the circumstance that these two extrinsic effects occur at different length scales (crack sizes). In this case, three independent parameters are required, two controlling the length scales and one weighting the two crack closure mechanisms. Whatever is the model, the determination of cyclic R-curve is not trivial, as many testing parameters can influence the results [57].

For the fracture mechanics-based fatigue life prediction under VA loading, a large number of models have been proposed in the literature, of which the accuracy depends on the specific load history [58–60]. This is because of the complexity of load sequence effects. For example, crack growth following a single overload determines a transient in the crack opening function, which has been the subject of many studies [61–64]. However, it is certainly more reliable, for many randomly loaded structures, to measure the crack growth rate determined by the application of a load history sampled from a certain spectrum, and relate it to the crack driving force parameter derived for a specific stress range, e.g. the root mean square, as done by Barsom [65,66]. By following this approach, the load sequence effects are only globally accounted for.

The present paper aims to present a probabilistic fatigue life prediction model for fatigue crack growing at the weld toe, starting from an initial defect or weld imperfection. The presented model is able to consider the difference in the fatigue crack growth rate and threshold condition of small and large cracks. The crack propagation is considered under CA and VA loading, using spectrum fatigue crack growth data from the literature. The inputs of the model and its epistemic uncertainty are estimated in a frequentist statistical framework. The correlations proposed from Chapetti [46] and Murakami [54,55] were used to model the build-up of the extrinsic effects on the threshold condition and the fatigue crack growth rate. For VA loading, the fatigue crack growth rate has been determined from experimental data available in the literature which were determined under random block loading. Different from random loading, in which the entire load history is randomized, a block of loading is generated creating a random sequence of reversal points, i.e. a random block having a predefined length. This random block is applied repetitively until failure. Therefore, the entire load history is not purely random. The data have been inferred using the proposed model and applied to predict the fatigue life of non-load carrying cruciform joints under the same type of loading.

2. Models and methods

2.1. SIF determination for CA loading

Only the first mode of opening of the crack is considered in this research. Therefore, the SIF reported here always refers to this opening mode.

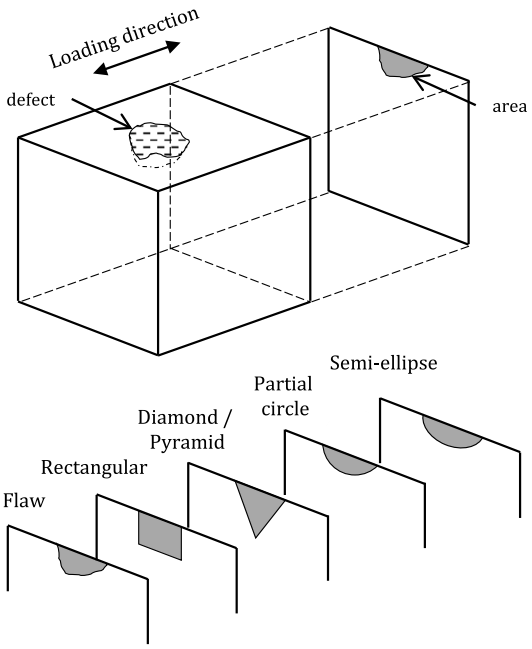

Fig. 4. Definition of the $\sqrt{area}$ parameter and the various types of surface defects investigated by Murakami [54].

In order to determine the fatigue crack growth rate using Eq. (18), the crack driving force is needed. The linear elastic SIF, K, is used as a crack driving force parameter, considering its wide applicability and the verified appropriateness to represent both small and long crack behavior, as mentioned in the introduction. At a given point along the crack front, the SIF is given by the sum of the SIFs obtained for primary (K_p) and secondary (K_s) stresses [67]:

$$K = K_p + K_s \tag{6}$$

The primary membrane and bending stresses are the nominal stresses obtained directly from the applied force and bending moment, respectively. The SIF for primary stresses is:

$$K_p = K_{p,m} + K_{p,b} \tag{7}$$

Because of the superposition principle, the SIF for primary loading is given by the sum of the SIF obtained under the membrane and bending components:

$$K_{p,m} = M f_w k_{tm} M_{wm} M_m \sigma_m \sqrt{\pi a} \tag{8}$$

$$K_{p,b} = M f_w k_{tb} M_{wb} M_b [\sigma_b + (k_m - 1)\sigma_m] \sqrt{\pi a} \tag{9}$$

where M is the bulging correction factor, f_w is the finite width correction factor, k_{tm} and k_{tb} are the membrane and bending stress concentration factors, M_{wm} and M_{wb} are the membrane and bending stress intensity magnification factors for the weld toe geometry, M_m and M_b are stress intensity magnification factors for membrane and bending, respectively, σ_m and σ_b are the membrane and the bending stresses, and k_m is the factor considering the effect misalignment. In Eqs. (8)–(9), the SIF is calculated using a generalization of the formula $K = Y\sigma\sqrt{\pi a}$, resulting from the Westergaard solution, in which Y is the geometry function, depending on the geometry, loading, and crack size, which is determined by the product of the factors M, M_m, M_b, M_k, k_t, k_m, and f_w, which are usually derived from finite element calculations, see compendia such as [67,68].

The secondary stresses, or residual stresses, are usually reported as normalized with respect to the yield stress, σ_y, and depend on the type of weldment. The SIF for secondary stresses is:

$$K_s = K_{s,m} + K_{s,b} + K_{s,sb} \tag{10}$$

In a similar way as for the primary stresses, the SIF for the secondary stresses is given by the sum of the SIF obtained using three components:

- the membrane component,

$$K_{s,m} = M_m \sigma_{s,m} \sqrt{\pi a} \tag{11}$$

- the bending component,

$$K_{s,m} = M_b \sigma_{s,b} \sqrt{\pi a} \tag{12}$$

- the self-balancing component,

$$K_{s,sb} = \sum_j (\sigma_j f_j) \sqrt{\pi a} \tag{13}$$

where σ_j is the jth coefficient of the stress distribution expressed as a polynomial function of the relative abscissa z/B, and f_j is the weight function. As for the primary stresses, Eqs. (11) and (12) express the SIF as in the Westergaard solution. A different approach is used in Eq. (13), where the weight function method [69] is used to calculate the SIF. Different from the geometric correction factors, the weight functions only depend on the geometry of the component and the size of the crack and are independent of the loading condition. Therefore, if the weight function for a cracked geometry is known, it is possible to compute the SIF for every type of load and crack size, given the nominal stress profile acting in the section where the crack is present. As mentioned, the stress profile is described with a polynomial relation as a function of the relative abscissa, z/B:

$$\sigma\left(\frac{z}{B}\right) = \sum_j \sigma_j \left(\frac{z}{B}\right)^j \tag{14}$$

where z is the distance between the considered point along the crack front and the free surface and B is the thickness of the section. The weight functions, f_j, can result from finite element calculation or can be found in handbooks or standards [67,70].

By considering both primary and secondary stresses, and for a load cycle in which bending and normal loading are in-phase, the SIF range, ΔK, and the load ratio, R, are given by:

$$\Delta K = K_{p,max} - K_{p,max} \tag{15}$$

$$R = \frac{K_{p,max} + K_s}{K_{p,max} + K_s} \tag{16}$$

2.2. Fatigue crack growth rate for small and long cracks

In accordance with the considerations made in [53], the fatigue crack growth rate for long cracks is modeled as a function of the SIF range, ΔK, the load ratio R, and the crack size a, using the Forman–Mettu equation modified as in [71]:

$$\frac{da}{dn} = C F_{lc} \Delta K^m \left(1 - \frac{\Delta K_{th}}{\Delta K}\right)^{p_{th}} \tag{17}$$

where C, p_{th}, and m are material constants, F is the crack velocity function, ΔK_{th} is the threshold of the SIF range. In [53] only the threshold of the SIF range is dependent on both the load ratio R, and the crack size a, whereas the crack velocity function is not. In particular, for a certain value of R the value of ΔK_{th} for small cracks is given by Eq. (2). In order to consider the effect of small cracks, also the crack velocity function needs to be modified, resulting in the following relationship:

$$\frac{da}{dn} = C F \Delta K^m \left(1 - \frac{\Delta K_{th}}{\Delta K}\right)^{p_{th}} \tag{18}$$

where F is the crack velocity function for small and long cracks. The effect of the crack size a, and the load ratio R, on the fatigue crack growth rate is depicted in Fig. 5, where the fatigue crack growth rate function resulting from Eq. (18) is qualitatively plotted together with the bounds of the fatigue crack growth rate in the Paris region and of the threshold of the stress intensity factor range. With increasing the crack size a:

- The threshold SIF range ΔK_{th} increases ranging between the intrinsic threshold $\Delta K_{th,eff}$, up to the value for long cracks $\Delta K_{th,lc}$.
- The fatigue crack growth rate in the Paris region decreases, ranging between the values obtained with and without considering crack closure.

By definition, these bounds are independent of the crack size. Increasing the load ratio R, determines that:

- The threshold SIF range decreases up to its intrinsic value $\Delta K_{th,eff}$.
- The fatigue crack growth rate in the Paris region increases up to the closure-free value.

The value of $\Delta K_{th,lc}$ and the lower bound of the fatigue crack growth rate are dependent on the load ratio R, since they are determined for long cracks, whereas $\Delta K_{th,eff}$ and the upper bound fatigue crack growth rate, i.e. under closure-free conditions, are independent on it.

For long cracks, the NASGROW model considers the extrinsic effects using the crack opening function given by:

$$f_{op} = \begin{cases} \max\{R; A_0 + A_1 R + A_2 R^2 + A_3 R^3\}, & \text{if } R \geq 0 \\ A_0 + A_1 R, & \text{if } R < 0 \end{cases} \tag{19}$$

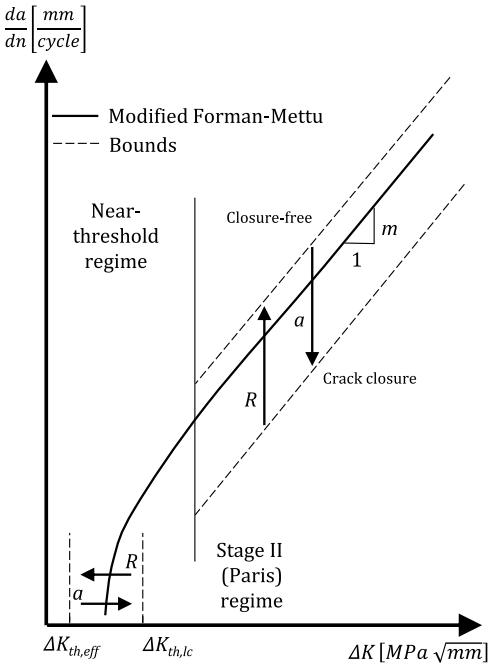

Fig. 5. Fatigue crack growth rate curve for long cracks and schematic effect of the crack size on the fatigue crack growth rate, Eq. (18).

where:

$$A_0 = (0.825 - 0.34\alpha + 0.05\alpha^2)\left[cos\left(\frac{\pi}{2}\frac{\sigma_{\max}}{0.5(\sigma_y + \sigma_u)}\right)\right]^{\alpha^{-1}} \tag{20}$$

$$A_1 = (0.415 - 0.071\alpha)\frac{\sigma_{\max}}{0.5(\sigma_y + \sigma_u)} \tag{21}$$

$$A_2 = 1 - A_0 - A_1 - A_3 \tag{22}$$

$$A_3 = 2A_0 + A_1 - 1 \tag{23}$$

where α accounts for the level of constraint, σ_y is the yield stress, and σ_u is the ultimate tensile strength. According to [53] the threshold SIF range for a long crack, $\Delta K_{th,lc}$, is:

$$\Delta K_{th,lc} = \Delta K_0\left(\frac{1 - f_{op}}{(1 - A_0)(1 - R)}\right)^{-(1+c_{th}R)} \tag{24}$$

where the coefficients of A_0, A_1 and c_{th} are calibration parameters, where c_{th} usually ranges between 0 and 3 if $R \geq 0$ or is approximately 0.1 if $R < 0$, α accounts for the level of constraint, and ΔK_0 is the threshold SIF range for long cracks at $R = 0$. In practice, the function that multiplies ΔK_0 takes into account the effect of plasticity induced crack closure, and it is a (monotonically decreasing) function of the load ratio.

To model the lower threshold SIF range and the higher crack growth rate that short crack exhibit with respect to long cracks, the threshold SIF range and the crack velocity function are modified to make explicit the dependence on the crack size. The build-up of the extrinsic effect related to long cracks, i.e. $\Delta K_{th,op,lc} = \Delta K_{th,lc} - \Delta K_{th,eff}$, is modeled as in [56]:

$$\Delta K_{th} = \Delta K_{th,eff} + (\Delta K_{th,lc} - \Delta K_{th,eff})[1 - \exp(-k(a - d))] \tag{25}$$

where d is the position from the surface of the strongest microstructural barrier, and k is a calibration parameter. In particular, d also stands for the crack size for which the effect of the microstructure is negligible. The parameter k controls the built-up of the extrinsic effect and the length scales at which this happens: $1/k$ represents a crack length at which a certain initial value of the extrinsic effect has decreased to $1/e$ of its initial value, where e is the Euler's number. Whereas d is only dependent on the material and its microstructure, k also depends on the load ratio, R. Chapetti [46] proposed the following relation for estimating k:

$$k = \frac{1}{4d}\frac{\Delta K_{th,eff}}{\Delta K_{th,lc} - \Delta K_{th,eff}} \tag{26}$$

which gave a good agreement with test data related to several metals including aluminum, steel, and copper.

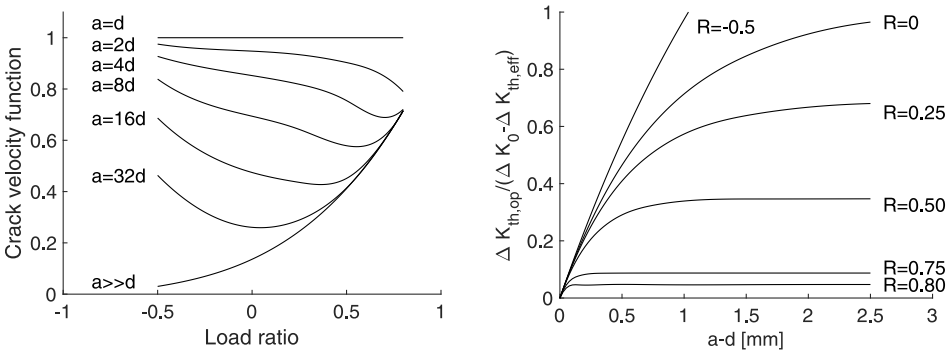

(a) Crack velocity function (b) Extrinsic component of ΔK_{th}

Fig. 6. Crack velocity function F, as a function of the load ratio R, for different crack sizes a (a), and the extrinsic component of the threshold of the SIF range normalized for its value at $R = 0$ as a function of $a - d$, for several values of the load ratio R (b).

In accordance with [53,72] the crack velocity function for long cracks, F_{lc}, is given by:

$$F_{\mathrm{lc}} = \left(\frac{1 - f_{\mathrm{op}}}{1 - R}\right)^{m} \tag{27}$$

where m is the exponent of the FCGR function. In a similar fashion as done by Maierhofer [41], the crack velocity function for small and long cracks is obtained by correcting F_{lc} using the exponential term in Eq. (25):

$$F = 1 - (1 - F_{\mathrm{lc}})[1 - exp(-k(a - d))] \tag{28}$$

Therefore, this model is able to represent the growth of small and long cracks growing from the critical location in weldments and propagating according to mode I loading, i.e. in a direction perpendicular to the direction of the maximum principal stress.

For the determination of ΔK_{th}, Eq. (25), and F, Eq. (28), for the point C, i.e. the intersection of the crack front with the free surface, see Fig. 1, the semi crack width c is used instead of the crack depth, a. This is based on the circumstance that the SIF is defined, for every point of the crack front, to quantify the stress intensification in the vicinity of the crack tip and in the plane perpendicular to the crack front.

The trend of the crack velocity function as a function of the load ratio for several values of the crack size is depicted in Fig. 6(a). Since the parameter k depends on the load ratio, R, and it is not a unique value, the trend of the crack velocity function F shown in Fig. 6(a) is not monotonic.

According to Eq. (26), at higher values of R, the reduction of the extrinsic component determines that the value of k increases. Therefore, a larger value of k in Eq. (25) implies that the extrinsic component, $\Delta K_{\mathrm{th,op}} = \Delta K_{\mathrm{th}} - \Delta K_{\mathrm{th,eff}}$, is fully established, i.e. $\Delta K_{\mathrm{th,op}} = \Delta K_{\mathrm{th,op,lc}}$, for smaller values of a than at lower values of the load ratio R. This is also visible in Fig. 6(b), where the extrinsic component of the threshold of the SIF range normalized for its value at $R = 0$ is shown as a function of the crack size for several values of the load ratio, R. It results that for lower values of R a larger crack depth a is required in order for the extrinsic component to be fully active, i.e. for $\Delta K_{\mathrm{th}} \approx \Delta K_{\mathrm{th,lc}}$. Instead, at higher values of R, the extrinsic component is fully developed for shorter crack depths.

3. Estimation of the model parameters and their uncertainty

3.1. Secondary stresses for CA and VA loading

Secondary stresses are of high importance for fatigue crack propagation, as they modify the load ratio, and in turn, the extent of plasticity induced crack closure. Positive residual stresses determine a higher fatigue crack growth rate and a lower threshold, forming therefore a more severe condition. Residual stress profiles at the weld toe can be obtained either through measurements or by finite element modeling, and in both cases the evaluation is non-trivial. In Fig. 7 the residual stress profile is depicted for different types of weldments. Based on these data, in [73] it is suggested that the mean value is:

$$\frac{\sigma_{\mathrm{s}}}{\sigma_{\mathrm{y}}} = 0.62 + 2.3267\frac{z}{B} - 24.125\frac{z}{B}^{2} + 42.485\frac{z}{B}^{3} - 21.087\frac{z}{B}^{4} \tag{29}$$

where σ_{y} is the yield stress. Eq. (29) does not strictly satisfy the self-equilibrium. However, it is here used to estimate the distribution of the residual stress state under CA loading, since it is believed to be the most accurate description of the trend of the residual stresses that is available. Despite in this work the residual stresses are not modeled in a probabilistic fashion, the variability encountered can be modeled in two ways, considering the description of the scatter proposed in [73], i.e. a normal distribution with mean value equal to one and a coefficient of variation equal to 0.25 at $z/B = 0$ (a standard deviation equal to 0.155). This

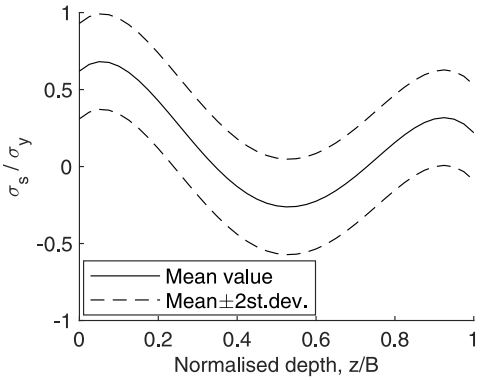

Fig. 7. Transverse residual stress profile for several types of weldments (T-butt, Plate on plate, T tubular, Y tubular) [5]. Scatterband and mean regression line, Eq. (29).

normal distribution can be used to either multiply only the first term of Eq. (29), or to multiply the outcome of Eq. (29). Whilst in the first way the self-balancing property of the residual stress distribution is not satisfied, in the second way the scatter resulting is not uniform as shown from the data reported in [5].

Under VA loading, the residual stresses that are plotted in Fig. 7 may be modified due to the application of stress peaks [74]. This causes shakedown of residual stresses, which are observed to strongly reduce in magnitude during cyclic loading [3]. This is the reason why, under VA loading, different modeling of the residual stresses is needed. The residual stresses to be used for VA loading can be estimated according to the indication based in BS7910 [67], Annex O. It is recommended that if the welded component is subjected to a proof load leading to limited plasticization in the cracked section, the residual stress state reduces to:

$$\sigma_s = \min\left\{ \sigma_y; \sigma_y \left[1.4 - \frac{\sigma_{ref}}{0.5(\sigma_y + \sigma_u)} \right] \right\} \tag{30}$$

where σ_{ref} is the reference stress due to the applied primary load. In the case of variable amplitude random block loading, the reference stress is calculated for every block.

Reference stress solutions are reported in standards, guidelines, and compendia [53,67,75]. For a semi-elliptical surface crack growing in a rectangular section, the reference stress for normal bending restraint, and for negligible bending restraint are respectively given by (BS7910):

$$\sigma_{ref} = \frac{\sigma_b + [\sigma_b^2 + 9\sigma_m^2(1-\alpha'')^2]^{0.5}}{3(1-\alpha'')^2} \tag{31}$$

$$\sigma_{ref} = \frac{\sigma_b + 3\sigma_m\alpha'' + [(\sigma_b + 3\sigma_m\alpha'')^2 + 9\sigma_m^2(1-\alpha'')^2]}{3(1-\alpha'')^2} \tag{32}$$

where

$$\alpha'' = \begin{cases} \frac{a/B}{1+B/c}, & \text{if } T_w \geq 2(c+B) \\ \frac{2ac}{BT_w}, & \text{if } T_w < 2(c+B) \end{cases} \tag{33}$$

where B and T_w are thickness and the width of the cross section of the crack. The maximum bending and membrane stress σ_b and σ_m are evaluated at the maximum stress range of the spectrum, that is $\Delta\sigma_{max}/(1-R)$. Eq. (30) is used to evaluate the relaxation of the residual stress following the application of $\Delta\sigma_{max}$ under VA loading, assuming that the residual stresses are uniformly distributed.

3.2. Cyclic R-curve

This section shows the proposed approach to estimate the cyclic R-curve according to Eq. (25) from [56]. To do so, the relationships of Murakami [54,55] and Chapetti [46] are used.

According to Murakami [54,55], for a load ratio $R = -1$, the fatigue limit of polished specimens of low to medium strength steels, is related to the Vickers hardness, H_V by:

$$\frac{\Delta\sigma_0}{2} = 1.6H_V \tag{34}$$

where $\Delta\sigma_0$ is the stress range at the fatigue limit. Eq. (34) applies to specimens which are assumed to be free of defects. In the case of specimens with defects, the threshold stress range, $\Delta\sigma_{th}$, for which crack propagation does not occur has been related also to the

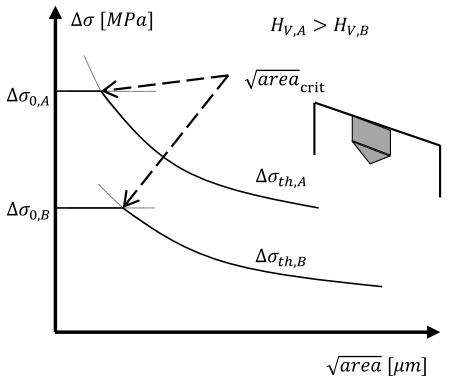

Fig. 8. Effect of a small drilled hole on the fatigue limit for two hypothetical steels (A and B), for which $H_{V,A} > H_{V,B}$. The size of the hole is expressed by the $\sqrt{area}$.

Vickers hardness and to the defect size. The size of the defect is accounted for by the $\sqrt{area}$ parameter introduced in Section 1, see Fig. 4. In this case, the relation also includes the dependency from the load ratio R:

$$\frac{\Delta\sigma_{th}}{2} = 1.43(H_V + 120)\sqrt{area}^{-1/6}\left(\frac{1-R}{2}\right)^{0.226+10^{-4}H_V} \tag{35}$$

where $\sqrt{area}$ is in μm. This relation was derived by introducing micro-defects of different sizes in polished specimens. For relatively small defect sizes, the threshold stress range was found to be equal to the fatigue limit. This leads to the definition of the critical value of the $\sqrt{area}$ parameter, i.e. $\sqrt{area}_{crit}$, indicating the largest defect size for which the propagation of the defect does not occur at any stress range lower than the fatigue limit. In other words, for $\sqrt{area} \le \sqrt{area}_{crit}$ the threshold stress is coincident with the fatigue limit and Eq. (35) is not valid, see Fig. 8. Therefore, if $\sqrt{area} < \sqrt{area}_{crit}$ the considered defect is smaller than the inherent defects inevitably present in the material, which dominate the phenomenon. Given the value of the Vickers hardness and considering $R = -1$, the value of $\sqrt{area}_{crit}$ can be estimated by equating Eqs. (34) and (35):

$$\sqrt{area}_{crit} = \left(\frac{1.43(H_V + 120)}{1.6H_V}\right)^6 \tag{36}$$

and is found to be decreasing with increasing the Vickers hardness.

The threshold condition for fatigue crack propagation expressed using the linear elastic crack driving force parameter, ΔK, is:

$$\Delta K_{th} = Y\Delta\sigma_{th}\sqrt{\pi\sqrt{area}} \tag{37}$$

where $\Delta\sigma_{th}$ is in MPa, and is estimated using Eq. (35), the geometry factor Y incorporates all the factors that were made explicit in Eqs. (8)–(9), and refers to surface cracks in smooth specimens. For small semi-circular surface cracks, as those observed to initiate in smooth specimens [23], $Y = 0.65$. Eq. (37) predicts the trend of the threshold of the SIF range as a function of the crack size, i.e. it is the cyclic R-curve proposed by Murakami. However, Eq. (37) does not asymptotically tend to $\Delta K_{th,lc}$, therefore it does not follow the expected trend of a cyclic R-curve that is depicted in Fig. 3, and it does not allow to predict the value of $\Delta K_{th,lc}$. To overcome this inconvenience, Eqs. (35) and (37) are considered valid up to approximately $\sqrt{area} = 1000$ μm [54,55]. However, as mentioned in Section 1, a crack cannot be defined as "short" or "long" through absolute length scales, therefore, the aforementioned upper limit of Eq. (37) is not used here to derive any correlation with $\Delta K_{th,lc}$. By making explicit Y and $\Delta\sigma_{th}$ in Eq. (37), it becomes:

$$\Delta K_{th} = 2 \cdot 0.65 \cdot 10^{-3}\left[1.43(H_V + 120)\sqrt{area}^{-1/6}\left(\frac{1-R}{2}\right)^{0.226+10^{-4}H_V}\right]\sqrt{\pi\sqrt{area}} \tag{38}$$

for the SIF expressed in [MPa $m^{0.5}$] and the $\sqrt{area}$ in [μm]. Fig. 9 depicts the typical trend of the cyclic R-curve of a material (continuous line), and the trend of the SIFs as a function of the crack size, of which the initial value is a_{ini}, under the effect of three stress ranges under constant amplitude loading (dashed line). The crack size is on the horizontal axis, whereas the SIF range is on the vertical axis. Starting from a crack of size d, the cyclic R-curve divides the region of propagating cracks $\Delta K > \Delta K_{th}$ from that one of non propagating cracks $\Delta K \le \Delta K_{th}$. A cyclic R-curve is conditional to the load ratio, R. According to Eq. (25), d is the size of the largest microstructural barrier from the free surface [46]. Each dashed curve in Fig. 9 relates the SIF range with the crack size for an applied stress range of constant amplitude. Three situations may occur: for $\Delta\sigma < \Delta\sigma_0$, the dashed line intersects the cyclic R-curve, estimating the size of the non propagating crack; for $\Delta\sigma > \Delta\sigma_0$ the dashed line does not intersect the cyclic R-curve, i.e. the crack potentially propagates until failure occurs; for $\Delta\sigma = \Delta\sigma_0$ the dashed line is tangent to the cyclic R-curve, also in this case

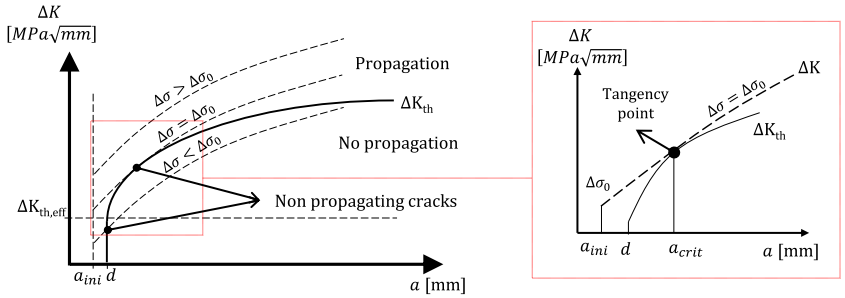

Fig. 9. Schematic of the cyclic R-curve. Effect of the applied stress range and simplification adopted with respect to approximation of d.

estimating the size of the non propagating crack. This condition is the same as predicted by Eq. (36). By considering the defect to be of semi-circular shape, the $\sqrt{area}_{\text{crit}}$ [μm] can be translated in terms of crack depth [mm]:

$$a_{\text{crit}} = \left(\frac{2(\sqrt{area}_{\text{crit}})^2}{\pi} \right)^{1/2} 10^{-3} \tag{39}$$

Therefore, the critical crack depth a_{crit}, i.e. the abscissa of the tangency point illustrated in Fig. 9, can be estimated using $\sqrt{area}_{\text{crit}}$, and the corresponding threshold of the SIF range, $\Delta K_{\text{th}}(\sqrt{area}_{\text{crit}})$, can be estimated using Eq. (38). In this work it is assumed that a_{crit} is a reasonable estimate of d, that can potentially be used if this quantity is not available. This assumption is going to be validated in the next section, by comparing the predicted cyclic R-curve with experimental data from literature. This assumption is based on two arguments: (1) these quantities are expected to be very close, mostly because of the trend of both the cyclic R-curve, i.e. the continuous line in Fig. 9, and the loading curve, i.e. the dashed line in Fig. 9; (2) the growth of non-propagating cracks before they stop ($\Delta\sigma \leq \Delta\sigma_0$) is not of interest for determining the fatigue life under CA loading, as also postulated in [29]. If a_{crit} is used instead of d, the relationship proposed by Chapetti [46], i.e. Eq. (26), to estimate k is here modified into:

$$k = \frac{1}{4a_{\text{crit}}} \frac{\Delta K_{\text{th,eff}}}{\Delta K_{\text{th,lc}} - \Delta K_{\text{th,eff}}} \tag{40}$$

Assuming that $d \sim a_{\text{crit}}$ also implies that $\Delta K_{\text{th,eff}}$ is approximated by the value of the threshold of the SIF range evaluated for $\sqrt{area}_{\text{crit}}$ by making use of Eq. (38). In this case, the dependency of the estimated value of $\Delta K_{\text{th,eff}}$ from the load ratio, R, is made explicit because the tangency point between the cyclic R-curve and the loading curve depicted in Fig. 9 inevitably depends on the load ratio R, since both $\Delta\sigma_0$ and $\Delta K_{\text{th,lc}}$ depend on it.

In summary, in the present work, the cyclic R-curve is modeled according to the exponential model of McEvily [56], which makes use of two calibration parameters, i.e. d and k. The distance of the first microstructural barrier from the free surface, d, is estimated using $\sqrt{area}_{\text{crit}}$ [54,55]. In order to estimate the parameter k, this leads to rewriting Eq. (26), initially proposed by Chapetti [46], into Eq. (40). By using the proposed procedure, the required inputs to estimate the cyclic R-curve are:

- the Vickers hardness H_{V}, which allows estimating $\sqrt{area}_{\text{crit}}$ and k,
- and the threshold SIF range for long cracks $\Delta K_{\text{th,lc}}$.

3.2.1. *Validation and estimation of the uncertainty for the threshold condition*

The aim of this section is to assess the accuracy of the predicted cyclic R-curve following the proposed approach described in the previous section, and to validate both the assumption of $d \sim a_{\text{crit}}$ and the applicability of Eq. (40).

For the present analysis, four approaches are considered to estimate the cyclic R-curve:

1. the model of Mc Evily [56], Eq. (25), and the proposed approach to estimate the parameters;
2. the model of Mc Evily [56], Eq. (25), and the correlations proposed by Chapetti [46] to estimate the parameters;
3. the model proposed in the FITNET, i.e. Eq. (2), based on the El-Haddad [52] approximation of the Kitagawa and Takahashi diagram [43];
4. the model of El-Haddad [52], using the correction proposed by Zerbst [29], and considering d as the initial crack size.

These approaches are also used for qualitative and quantitative comparison with experimental data available from the scientific literature. The test data from four different steels are reported in [46], and are used for the validation of the proposed approach. With respect to each dataset, the inputs are summarized in Table 1.

In the proposed approach, the value of H_{V} is estimated from $\Delta\sigma_0$ using Eq. (34). It allows estimating $\Delta K_{\text{th,eff}}$, which is approximated by Eq. (38) for $\sqrt{area} = \sqrt{area}_{\text{crit}}$, the latter estimated using Eq. (36). The value of a_{crit} is estimated using Eq. (39), allowing k to be determined by Eq. (40). The only required quantity is $\Delta K_{\text{th,lc}}$ that for the current analysis is reported in Table 1. The approach proposed by Chapetti [46] makes use of the measured values of d, $\Delta K_{\text{th,lc}}$ and $\Delta K_{\text{th,eff}}$, which are reported in Table 1. The approach reported in the FITNET guideline [53] makes only use of $\Delta K_{\text{th,lc}}$, reported in Table 1. The correction factor proposed

Table 1
Datasets considered for the validation, $R = -1$ and $\sigma_s = 0$.

Steel grade	d [mm]	$\Delta\sigma_0$ [MPa]	$\Delta K_{th,eff}$ [MPa m$^{0.5}$]	$\Delta K_{th,lc}$ [MPa m$^{0.5}$]	Ref.
0.42 C	0.018	450	2.2	5.9	[76]
2.25Cr1Mo	0.025	500	2.9	9.1	[77]
S20 C	0.0078	470	1.5	10.4	[78]
S20 C	0.055	326	2.8	12.4	[78]

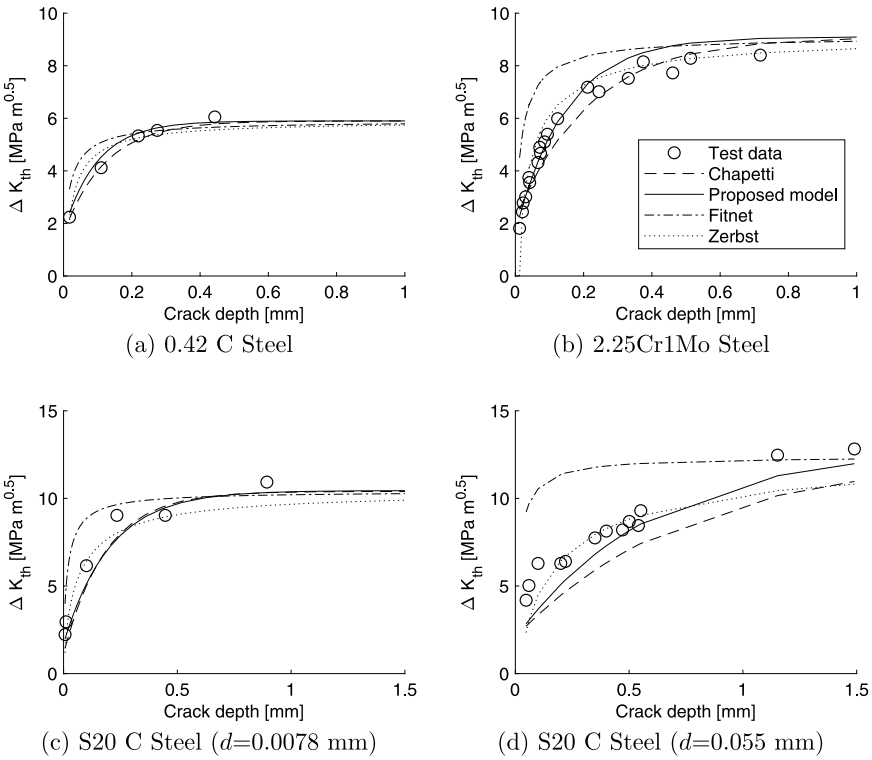

Fig. 10. Cyclic R-curve. Comparison between test data, see Table 1, and the four approaches considered in the present paper.

by Zerbst [29], and the intrinsic crack length are both estimated using the material properties reported in Table 1. Moreover, the crack extension is calculated as $a - d$.

The comparison between the four approaches and the test data is depicted in Fig. 10. It results that the current approach leads to a cyclic R-curve well in agreement with test data, similar to the approaches proposed by Chapetti [46] and Zerbst [29]. However, the current approach requires fewer material properties to be measured. Instead, the El-Haddad approximation as proposed in the NASGROW model leads, in every examined case, to an evident overestimation of the cyclic R-curve. Therefore, it is not considered for further analyses.

Fig. 11a shows a box plot diagram of the residuals of the experimental threshold SIF range vs. the model prediction where the single data reported are considered as outliers. The residuals are calculated as the difference between the logarithm of the predicted threshold SIF range vs. the logarithm of the experimental threshold SIF range. It can be deduced that the proposed approach determines a coefficient of variation equal to 0.1, similar to the approach proposed by Zerbst. By analyzing the residuals resulting from the approach proposed by Chapetti, it can be seen that this approach leads to a less severe threshold condition than the test data, and the distribution of the residuals is more scattered. On the contrary, the residuals resulting from the FITNET approach determine a more severe threshold condition than the data, and show a significantly larger scatter and bias. Fig. 11b shows the normal probability plots for the same residuals, highlighting that the results of the proposed approach and that one from Zerbst determine a less biased and scattered distribution than the other approaches. Moreover, the p-values resulting from the Shapiro–Wilk test for normality [79] are 0.95, 0.033, $0.53 \cdot 10^{-5}$, and 0.11 for the approaches proposed here, by Chapetti, by Zerbst and by the FITNET recommendation, respectively. This means that for a (widely used) significance level of 0.05 the null hypothesis of the Shapiro–Wilk test is rejected for the results produced by using the approaches proposed by Chapetti and Zerbst. For the approach of Zerbst, this is due to the tail of the data which, according to Fig. 11b, is not matching with the assumed normal distribution (see the purple data for a probability exceeding 0.90). Moreover, the residuals resulting from the proposed approach

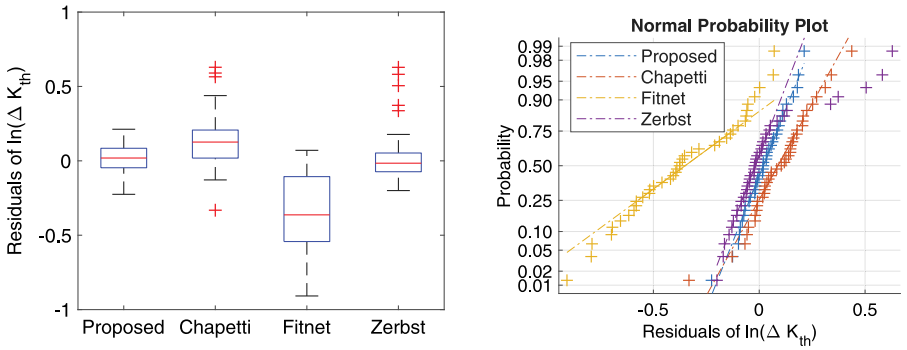

(a) Box plot (b) Normal probability plot

Fig. 11. (a) Box-plot diagram identifying the inter quartile range and prediction bounds of the residuals, and (b) Normal probability plot of the residuals. (For interpretation of the references to color in this figure legend, the reader is referred to the web version of this article.)

Table 2
Estimation of the aleatory and epistemic uncertainties for the parameters of the model proposed by Murakami, and the estimation of the variability of the fatigue limit according to [81].

Parameter	Estimator	St.err.	Correlation matrix			
α_1	3.30E−03	8.18E−05	1	−4.58E−01	−7.06E−01	−3.56E−01
α_2	120	5.49E+00	–	1	−2.78E−01	2.34E−01
α_3	0.33	4.60E−03	–	–	1	2.03E−1
$\sigma_{ln(\Delta K_{th})}$	0.05	1.42E−03	–	–	–	1
$\Delta\sigma_0$	1.6 H_V	0.14	See [81]			

are more in accordance with a normal distribution than for the FITNET, this is because the larger the p-value is, the more it supports the null-Hypothesis of the test.

Therefore, the authors consider the proposed approach as preferable, because of three reasons: (1) it appears to be less biased, (2) leads to a less scattered distribution of the log-residuals, and (3) it requires fewer input variables. In particular, it requires only the Vickers hardness, which can be easily measured, and the threshold of the SIF range for long cracks, which can be measured relatively easy, e.g. in comparison to $\Delta K_{\text{th,eff}}$, and is reasonably known for many steel grades.

3.2.2. Estimation of the uncertainty for the correlation between $\sqrt{area}$ and ΔK_{th}

From the previous section it follows that the correlations developed by Murakami are used to estimate relevant quantities such as $\Delta K_{\text{th,eff}}$ and a_{crit}. In order to consider the uncertainty resulting from the use of these correlations, the test data used from Murakami are re-analyzed using the maximum likelihood method.

The relation expressed by Eq. (38) reduces, by multiplying all the constants, into:

$$\Delta K_{\text{th}} = 3.3\,10^{-3}(H_V + 120)\sqrt{area}^{1/3}\left(\frac{1-R}{2}\right)^{0.226+10^{-4}H_V} \quad [\text{MPa m}^{0.5}] \tag{41}$$

For a load ratio $R = -1$, the previous equation results in the relationship reported in [54]:

$$\Delta K_{\text{th}} = 3.3\,10^{-3}(H_V + 120)\sqrt{area}^{1/3}\,[\text{MPa m}^{0.5}] \tag{42}$$

The $\sqrt{area}$ parameter is expressed in [μm]. This equation has been obtained by fitting test data obtained from smooth specimens containing defects. The data related the size of the defect, using the $\sqrt{area}$ parameter, to ΔK_{th}. The regression model associated with Eq. (42) is as follows:

$$\Delta K_{\text{th}} = \alpha_1(H_V + \alpha_2)\sqrt{area}^{\alpha_3} + \epsilon \tag{43}$$

and ΔK_{th} is assumed to be distributed according to a log-normal distribution. The maximum likelihood method [80] is used to infer the experimental data with the aim of estimating the uncertainty.

The estimators of the model parameters α_1, α_2, α_3, and the standard deviation of the log-residuals $\sigma_{ln(\Delta K_{\text{th}})}$ are reported in Table 2 together with the standard error and the correlation matrix obtained from the Fisher information matrix of the likelihood function. The epistemic uncertainty are modeled using a multivariate normal distribution having as a location parameter the estimator of the model parameters. The covariance matrix can be obtained from the standard error and the correlation matrix, both reported in Table 2. These results can be used in a probabilistic assessment in which d and $\Delta K_{\text{th,eff}}$ are estimated using the procedure proposed in this paper. The estimators of the parameters are coincident with those proposed by Murakami [54,55]. Moreover, the estimated

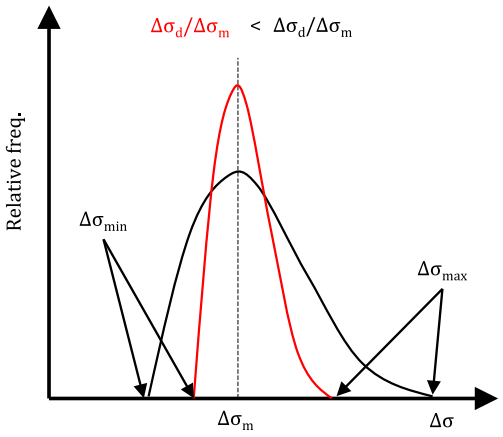

Fig. 12. Rayleigh spectrum with truncation at $\Delta\sigma_{max}$.

standard error is always relatively small as compared to the estimator, <1%. This is associated with the relatively large number of data. The quantities in Table 2 can be used to consider epistemic and aleatory uncertainty underlying the approach proposed by Murakami.

3.3. Fatigue crack growth rate under VA loading

In this section, the fatigue crack growth rate data from [66] resulting from the application of the Rayleigh stress spectrum is inferred using the fatigue crack growth rate model proposed in Section 3.3.1. The results of the fit and the model parameters are discussed in Section 3.3.2.

3.3.1. Model for inferring fatigue crack growth rate data obtained for VA random block loading

The model proposed for fatigue crack growth under VA random block loading is based on fatigue crack growth data obtained by applying a stress history in which the relative frequency of occurrence of a stress range follows the truncated Rayleigh distribution function and the load ratio R is fixed. The truncated Rayleigh distribution is depicted in Fig. 12, where the effect of the modal stress range $\Delta\sigma_m$ and the dispersion stress range $\Delta\sigma_d$, is shown. In the majority of the experimental studies performed by making use of this type of load spectrum [65,66], and based on the analyses of Klippstein [82], the truncation was applied at $\Delta\sigma_{max} = \Delta\sigma_m + 2\Delta\sigma_d$, and $\Delta\sigma_{max} = \Delta\sigma_{min} + 3\Delta\sigma_d$. For this type of VA loading, Barsom [65] demonstrated that in the Paris region the fatigue crack growth rate can be correlated with that one resulting from CA loading tests. In particular, a very good agreement was found when plotting the fatigue crack growth rate against the root-mean-square SIF range ΔK_{rms} for CA and VA data (despite the lack of a physical meaning of the root-mean-square SIF). Therefore, this is here used merely as a correlation.

The VA fatigue crack growth data in the near-threshold region produced by Fisher for A36 steel [66] are used in this paper in order to relate a characteristic value of the SIF range to the measured fatigue crack growth rate. The test data were produced by monitoring fatigue crack growth in central crack specimens, subjected to repeated blocks of a random load history sampled from the truncated Rayleigh distribution shortly described before. Three load ratios were used: 0.3, 0.55, and 0.80. In every case, $\Delta\sigma_{min} = 0$, and the ratio $\Delta\sigma_d/\Delta\sigma_m$ was kept equal to 1.

Since most of the crack propagation time of as-welded details is spent in the near-threshold region as a small fatigue crack, accurate modeling of the near-threshold fatigue crack growth rate is crucial. Different from [65,66] the maximum SIF range, ΔK_{max}, resulting from the maximum stress range of the spectrum, $\Delta\sigma_{max}$, is used as a crack driving force to correlate the threshold condition under CA and VA loading. This is because, under spectrum loading, the crack is assumed to propagate if $\Delta K_{max} > \Delta K_{th}$. For what concerns the Paris region, the correlation found by Barsom is used. For the estimation of ΔK_{th} and the near threshold fatigue crack propagation, the VA fatigue crack growth rate data in [66] will be useful to validate these hypotheses and, at the same time, gain an understanding of the near-threshold fatigue crack growth rate.

The proposed fatigue crack growth model is based on Eq. (18). However, the relations to describe the dependency of $\Delta K_{th,lc}$ on the load ratio, Eq. (24), and the crack velocity function, Eq. (27), although remaining similar to those of the NASGROW model [53] are modified into:

$$\Delta K_{th,lc,\Omega} = \Delta K_{0,\Omega}\left(\frac{1 - f_{op,\Omega}}{(1 - B_0)(1 - R)}\right)^{-(1+R\gamma_{th})} \tag{44}$$

$$\Delta K_{eff}^{m_\Omega} = \Delta K^{m_\Omega} F_{lc,\Omega} \quad \text{where } F_{lc,\Omega} = \left(\frac{1 - R}{1 - f_{op,\Omega}}\right)^{m_\Omega} \tag{45}$$

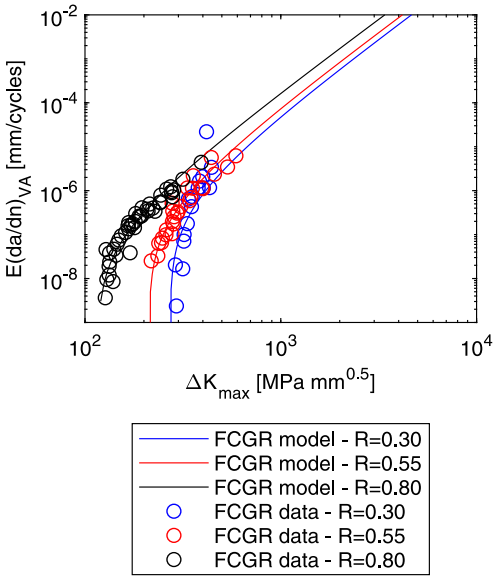

Fig. 13. Spectrum fatigue crack growth rate data, fit using the proposed model.

The crack opening function $f_{\mathrm{op},\Omega}$, related to spectrum is expressed similar to that one of the NASGROW model [53], but simplified with respect to Eq. (19):

$$f_{\mathrm{op},\Omega} = \max\{R; B_0 + B_1 R\} \tag{46}$$

The variables $\Delta K_{0,\Omega}$, B_0, B_1, γ_{th} are model parameters that are estimated based on fatigue test data. $F_{lc,\Omega}$ represents the crack velocity function for long cracks related to the considered spectrum Ω, and $\Delta K_{\mathrm{th},lc,\Omega}$ is the threshold SIF range for long cracks related to the spectrum Ω for which, if $\Delta K_{\max} > \Delta K_{\mathrm{th},lc,\Omega}$ fatigue crack propagation is assumed to occur. As for the CA loading, γ_{th} is assumed to be equal to 2. Therefore, for long cracks Eq. (18) becomes:

$$E\left[\frac{da}{dn}\right]_{\mathrm{VA}} = C_\Omega F_{lc,\Omega} \Delta K_{\max}^{m_\Omega} \left(1 - \frac{\Delta K_{\mathrm{th},lc,\Omega}}{\Delta K_{\max}}\right)^{p_{\mathrm{th},\Omega}} \tag{47}$$

where $E\left[\frac{da}{dn}\right]_{\mathrm{VA}}$ is the averaged fatigue crack growth rate resulting from the application of the spectrum, C_Ω, m_Ω, and $p_{\mathrm{th},\Omega}$ are the model parameters for random block VA loading. The parameter m_Ω can be assumed equal to m resulting from CA loading. The parameters $p_{\mathrm{th},\Omega}$, and C_Ω depend on the specific value of $\Delta\sigma_{\mathrm{d}}/\Delta\sigma_{\mathrm{m}}$, i.e. their values depend on the specific spectrum, because of the load sequence effects.

3.3.2. Estimation of the uncertainty for the fatigue crack growth rate under VA random block loading

In this section, the VA fatigue crack growth rate data from [66] are inferred using the model proposed in the previous section. The aforementioned data were obtained by testing central crack specimens and applying a VA random block loading of which the stress spectrum follows the truncated Rayleigh distribution as introduced in the previous section. The agreement between the proposed fatigue crack growth rate model and the data is depicted in Fig. 13. In addition, the estimators of the parameters of the model and the resulting uncertainty are reported in Table 3. The analysis results in a very large standard error for $log_{10}(C_\Omega)$. This is attributed to the lack of fatigue crack growth rate data in the Paris region, as can be seen in Fig. 13. This large uncertainty is further amplified by the uncertainties of B_0, and B_1, of which the source is again the lack of data in the Paris regime. On the contrary, the estimator of $\Delta K_{0,\Omega}$ is very close to the values of ΔK_0 reported in [53] for similar steel grades. This supports the choice of using the value of $\Delta K_{\max}$ as crack driving force parameter for VA fatigue crack growth rate, with the aim of correlating the threshold condition for VA loading to that one obtained from CA fatigue crack growth rate data. For what concerns the near-threshold VA fatigue crack growth rate, it results that a smoother transition between the Paris regime and the threshold is obtained for the VA fatigue crack growth rate as compared to the CA fatigue crack growth rate. Indeed, the absolute value of the estimator of $p_{\mathrm{th},\Omega}$ (1.21), see Table 3, is larger than the absolute value of p_{th}, usually equal to 0.5 [53].

4. Results of the fatigue life prediction

The fatigue crack growth model described in Section 2.2 is used for two purposes. At first, a sensitivity analysis is carried out with the purpose of establishing the importance of the different parameters with respect to the predicted fatigue life and fatigue limit.

Table 3
Estimators and uncertainty of the parameters of the proposed model fitting the fatigue crack growth rate data from [66] obtained under spectrum loading.

Parameter			Correlation matrix						
Name	Estimator	St. Err.	m_Ω	$\sigma_{log_{10}(C_\Omega)}$	$\Delta K_{0,\Omega}$	$\sigma_{log_{10}(\Delta K_{0,\Omega})}$	$p_{th,\Omega}$	B_0	B_1
$log_{10}(C_\Omega)$	−1.39E+01	3.17E+00	−3.29E−01	−3.94E−02	−2.32E−02	−6.55E−02	−9.52E−02	9.55E−01	−9.54E−01
m_Ω	3.47E+00	3.74E−01	1.00E+00	1.62E−01	2.77E−01	2.37E−02	4.74E−01	−3.47E−02	3.22E−02
$\sigma_{log_{10}(C_\Omega)}$	2.37E−01	2.28E−02	–	1.00E+00	1.50E−01	−2.15E−01	3.23E−02	8.95E−03	−9.95E−03
$\Delta K_{0,\Omega}$	2.78E+02	1.34E+01	–	–	1.00E+00	−6.75E−01	7.72E−01	7.25E−02	−7.42E−02
$\sigma_{log_{10}(\Delta K_{0,\Omega})}$	2.92E−02	7.65E−03	–	–	–	1.00E+00	−4.01E−01	−6.68E−02	6.74E−02
$p_{th,\Omega}$	−1.21E+00	2.34E−01	–	–	–	–	1.00E+00	6.44E−02	−6.58E−02
B_0	3.66E−01	1.26E+00	–	–	–	–	–	1.00E+00	−9.90E−01
B_1	5.68E−01	1.13E+00	–	–	–	–	–	–	1.00E+00

Table 4
Reference values for the sensitivity analysis.

Parameter	Value		Ref.
$\Delta K_{th,eff}$	63	[MPa mm$^{0.5}$]	[67]
ΔK_0	278	[MPa mm$^{0.5}$]	[53,84]
a_{crit}	0.05	[mm]	[a]
a_{ini}	0.15	[mm]	[85]
a_{ini}/c_{ini}	0.62	[–]	[85]
C	2.50E−13	[b]	[84]
R	0.5	[–]	Ref.

[a] Arbitrary value.
[b] For da/dn in [mm], given ΔK in [MPa mm$^{0.5}$].

Secondly, the model is applied to a cruciform joint geometry under constant and variable amplitude loading, aiming to verify the agreement between the fatigue life prediction and the test data. The fatigue test data used for the validation are obtained from [83] and are related to a non-load carrying cruciform joint.

4.1. Sensitivity analysis for CA loading

The sensitivity analysis is carried out in order to determine the relative importance of each variable. The change of the response of the model is quantified after a separate perturbation of each of the variables. The semi-elliptical surface crack is considered to grow at the weld toe of a cruciform joint until its depth reaches 0.8 times the plate thickness, B. The variables considered in the sensitivity analysis are:

1. the intrinsic threshold $\Delta K_{th,eff}$,
2. the threshold for a long crack at $R = 0$, ΔK_0,
3. the estimated distance from the surface of the first microstructural barrier a_{crit},
4. the initial crack size a_{ini}
5. the initial crack aspect ratio a_{ini}/c_{ini},
6. the coefficient C of the crack growth rate law,
7. the load ratio R.

The monitored response of the model consists of three aspects: (1) the predicted fatigue limit $\Delta\sigma_0$, (2) the predicted fatigue life at $\Delta\sigma$ = 200 MPa, and (3) the predicted fatigue life at $\Delta\sigma$ = 300 MPa. For the fatigue life and the fatigue limit, respectively, the indicators of importance are defined as:

$$\eta_{N,\theta_i} = \frac{N_{\theta_i+\Delta\theta_i} - N_{\theta_i-\Delta\theta_i}}{N_{\theta_i}} \tag{48}$$

$$\eta_{\Delta\sigma_0,\theta_i} = \frac{\Delta\sigma_{0_{\theta_i+\Delta\theta_i}} - \Delta\sigma_{0_{\theta_i-\Delta\theta_i}}}{\Delta\sigma_{0_{\theta_i}}} \tag{49}$$

where N_{θ_i} is the number of cycles to failure predicted for the considered parameter θ_i to be equal to the reference value, $N_{\theta_i\pm\Delta\theta_i}$ are the number of cycles to failure predicted for the perturbed value. The same definition applies to the fatigue limit, $\Delta\sigma_0$. Each parameter is perturbed by 10%, i.e. $\Delta\theta_i = 0.1\theta_i$. The reference value of each parameter is reported in Table 4 and is based on typical values for structural steels.

For the purpose of carrying out the sensitivity analysis, the intrinsic threshold, $\Delta K_{th,eff}$, the cyclic R-curve, and the effect of the secondary stresses on the load ratio R are not evaluated as described in Section 3.2. This means that, the values of a_{crit} and $\Delta K_{th,eff}$ are directly assumed, instead of estimating them through the use of the H_V, in order to measure the influence of the distance of

Table 5
Result of the sensitivity analysis.

Input	Output		
θ_i	$\eta_{\Delta\sigma_0,\theta_i}$	η_{N,θ_i} at $\Delta\sigma$ = 200 MPa	η_{N,θ_i} at $\Delta\sigma$ = 300 MPa
$\Delta K_{\text{th,eff}}$	0.17	0.05	0.03
ΔK_0	0.05	0.02	0.01
d	−0.06	−0.03	−0.02
a_{ini}	−0.03	−0.09	−0.09
a_{ini}/c_{ini}	0.00	0.01	0.01
C	0.00	−0.20	−0.20
R	−0.02	−0.08	−0.08

Table 6
Mean values of the fatigue crack growth rate exponent and coefficient.

Material	C	m	Ref
S355	$4.96\,10^{-14}$	3.23	[87]
Mild steel weld	$1.83\,10^{-13}$	3.00	[88]
Mild steel weld	$2.50\,10^{-13}$	3.00	[84]
Mild steel weld	$1.09\,10^{-13}$	3.10	[89]
HAZ and BS958 steel	$8.78\,10^{-13}$	2.80	[90]

For da/dn in [mm], given ΔK in [MPa mm$^{0.5}$].
Closure free value assumed equal to the estimator at Re = 0.75.

the microstructural barrier and the intrinsic threshold of the SIF range on the fatigue strength and life. The resulting values of η_{N,θ_i} and $\eta_{\Delta\sigma_0,\theta_i}$ are reported in Table 5.

It clearly results that, given the reference values of the model parameters, the most dominant variables with respect to the estimation of the fatigue limit are $\Delta K_{\text{th,eff}}$ and d, but the effect is opposite (opposite sign). The third most important parameter is the threshold for long cracks at $R = 0$, ΔK_0. With respect to the predicted life at $\Delta\sigma$ = 200 and at $\Delta\sigma$ = 300 MPa, the most relevant parameters are the coefficient of the fatigue crack growth rate function, C, and the initial crack depth, a_{ini}. The effect of the load ratio R affects both the estimation of the fatigue limit and the fatigue life, because of the effect induced on ΔK_0, $\Delta K_{\text{th,eff}}$, and C. The variables that are more relevant for the threshold condition, ΔK_0, $\Delta K_{\text{th,eff}}$, and d determine a decreasing relevance with respect to the fatigue life with increasing the applied stress range. However, it must be noted that the results are based on an equal, independent, perturbation of all the parameters. In reality, standard deviations of these variables are different and, therefore, it is expected that a different ranking occurs if other methods, such as the First Order Reliability Method (FORM) are used.

4.2. Model validation for CA loading

The results of the proposed model are here graphically compared to a CA fatigue test dataset of cruciform joints obtained from [83].

The steel grade used was ASTM A572 Grade 50, equivalent to S235 steel for which the statistics of the monotonic tensile properties are investigated in [85,86]. The Vickers hardness was obtained from the Brinell hardness by using commonly available conversion tables. During fatigue crack propagation, the crack front might be located in the base material or in the coarse- or fine-grained heat-affected zone (HAZ), depending on the crack size and location. The prediction is performed using several fatigue crack growth rate exponents and coefficients available in standards, codes and literature. These values are reported in Table 6. The values in [87] are obtained for the base material of the S355 steel. The values reported in DVNGL-C201 [88], OTH 511 report [84], and DNV standard [89] refer to structural steel welds, whereas the values reported from [90] refer to HAZ in mild steels and BS958 steel grade from [91]. Table 7 summarizes the dataset and the dimensions of the welded detail tested in [83].

In order to determine the crack driving force, the geometry correction factors in Eqs. (6) and (7) are calculated using the equations reported in BS7910 [62]. In particular, the 3D solutions for calculating M_k are used. The final crack size is set equal to 0.8 times the thickness of the cross-section, which is the limit of validity for the equations used to calculate the geometry correction factors. According to [70], the geometry is considered to be subjected to membrane stress only, therefore $\sigma_b = 0$. A minimum stress equal to 13.8 MPa was applied, independent of the stress range. The residual stress distribution is assumed to follow Eq. (21).

Comparison is made between the predicted fatigue life using the proposed model, the prediction obtained using the models in the BS7910, and the experimental data obtained for CA loading.

The models in BS7910 make use either of a “simplified law”, i.e. the Paris law with threshold condition, or of a “bilinear law”, and a threshold of the SIF range independent of the load ratio, R. This is because the residual stress state is taken into account by considering the threshold of the SIF range for high load ratio, i.e. R larger than 0.5. Concerning the threshold condition, the standard recommends that for $a \geq 1$ mm the value, ΔK_{th} = 63 MPa mm$^{0.5}$, is a lower bound. However, it also recommended not to consider larger values of the threshold SIF range for $a < 1$ mm. The probabilistic model code of the JCSS [85] recommends a mean value: ΔK_{th} = 140 MPa mm$^{0.5}$, which is in accordance with the data reported in [84]. Given these indications, and the order

Table 7
Geometry, summary of the fatigue test data and input values of the models variables for comparison with the selected CA fatigue test data.

Geometry of the cruciform joint.					
Parameter		Value	Unit	Note	Ref.
Plate thickness	B	10	[mm]		[83]
Plate width	T_w	50	[mm]		[83]
Weld toe leg	Z	6	[mm]		[83]
Summary of fatigue test data.					
Failure data		20			[83]
Runout data		9			[83]
Inputs of the fatigue crack growth models — mean values					
Parameter		Value	Unit	Note	Ref.
U.T.S.	σ_u	555	[MPa]		[85,86]
Yield stress	σ_y	436	[MPa]		[85,86]
Brinell hardness	H_b	144	[–]		[81]
Vickers hardness	H_V	146	[–]		[a]
Long crack threshold	ΔK_0	278	[MPa mm$^{0.5}$]	[d]	[53]
FCGR parameter	p_{th}	0.5	[–]	[a]	[53]
FCGR parameter	α	2	[–]	[a]	[53]
FCGR parameter	c_{th}	2	[–]		[53]
Initial crack depth	a_{ini}	0.15	[mm]	[a]	[85]
Initial crack aspect ratio	a_{ini}/c_{ini}	0.62	[–]	[a]	[85]
Bilinear FCGR coefficient	C_1	4.80E−18	[b]		[84]
Bilinear FCGR coefficient	C_2	5.86E−13	[b]		[84]
Bilinear FCGR exponent	m_1	5.10	[–]		[84]
Bilinear FCGR exponent	m_2	2.88	[–]		[84]
Simplified FCGR coefficient	C_P	2.50E−13	[b]		[84]
Simplified FCGR exponent	m_P	3	[–]		[84]
Threshold SIF	ΔK_{th}	see Eq. (50)	[MPa mm$^{0.5}$]	[e]	[67]

[a] ASTM conversion table.
[b] For da/dn in [mm], given ΔK in [MPa mm$^{0.5}$].
[c] Closure free value assumed equal to the estimator at R = 0.75.
[d] Assumed for similar steel grade.
[e] To be used only for the models in BS7910 and for structural steels.

of magnitude of the initial crack depth considered in this work, the threshold condition for the models in BS7910 is assumed in this work as:

$$\Delta K_{th} = \begin{cases} 63, & \text{for } a < 1 \\ 140, & \text{for } a \geq 1 \end{cases} \tag{50}$$

which corresponds to a stepwise R-curve. The fatigue crack growth rate coefficients are independent on the crack depth and considered for load ratio R larger than 0.5. The input values are summarized in Table 7.

The results of the prediction are plotted in Fig. 14, where a good agreement can be observed between fatigue test data and the prediction of the proposed model. The best agreement results from the application of the fatigue crack growth rate coefficient and exponent proposed in [87], since it minimizes the sum of the residuals squared.

When compared to the prediction obtained using the BS7910, the fatigue life predicted using the proposed model is less conservative both in the finite life regime and at the fatigue limit, showing a better agreement with CA fatigue test data. The predicted fatigue life obtained by making use of the simplified law in the BS7910 is conservative with a factor of 3, at relatively low stress ranges. By using the bilinear law, the prediction is less conservative. Both models predict a significantly lower fatigue limit as compared to the CA fatigue test data. Instead, the proposed model predicts a fatigue limit more in line with the trend of the CA fatigue test data.

4.3. Model validation for VA loading

For the purpose of evaluating the model response for variable amplitude fatigue test data, the VA fatigue crack growth rate equation proposed in Section 3.3.1, Eq. (47), is applied. In this case, the residual stress state is assumed to be uniform, i.e. independent of z/B, and re-estimated every 500 cycles by making use of Eq. (30), since the block length applied in [83] for the production of the fatigue test data is 500 cycles. Furthermore, the model is applied a second time without considering the effect of the residual stresses. The first case is expected to give conservative results, because BS7910 is a design standard, whereas the second case is expected to provide a too optimistic prediction.

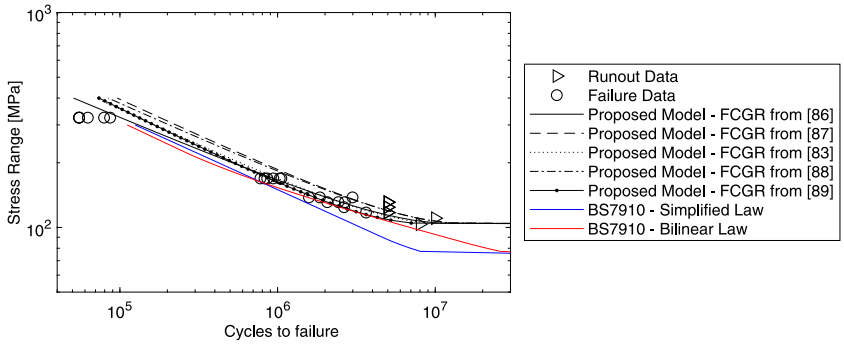

Fig. 14. Comparison between model prediction and fatigue test data under CA loading from [83].

The experimental results reported in [65] showed that, under a Rayleigh spectrum loading, the use of the root mean square of the SIF range, ΔK_{rms}, well correlates CA and VA fatigue crack growth rate data in the Paris region. This means that in the Paris region the average fatigue crack growth rate under this specific type of VA loading spectrum, can be estimated by:

$$E\left[\frac{da}{dn}\right]_{\mathrm{VA}} = C\Delta K_{\mathrm{rms}}^{m} \tag{51}$$

where C and m are respectively the fatigue crack growth rate coefficient and exponent for CA loading. This correlation was verified for several structural steels: A36, A588GrA, A588GrB, A514Gr.E, A514Gr.F.

The proposed model makes use of the maximum value of the SIF range, implying that Eq. (51) cannot be directly used. However, given the relationship between ΔK_{rms} and ΔK_{max}, it is possible to estimate the value of C_{Ω}. In light of the characteristics of the Rayleigh spectrum, ΔK_{max} can be related to ΔK_{rms}. In particular, for a Rayleigh spectrum truncated as in [83], that is $\Delta\sigma_{\mathrm{max}} = \Delta\sigma_{\mathrm{min}} + 3\Delta\sigma_{\mathrm{d}}$ (or equivalently $\Delta\sigma_{\mathrm{max}} = \Delta\sigma_{\mathrm{m}} + 2\Delta\sigma_{\mathrm{d}}$, because the data in [83] were produced using a Rayleigh spectrum having $\Delta\sigma_{\mathrm{d}}/\Delta\sigma_{\mathrm{m}} = 1$), it results that:

$$\Delta\sigma_{\mathrm{rms}} = \Delta\sigma_{\mathrm{m}} + 0.387\Delta\sigma_{\mathrm{d}} \tag{52}$$

Using the SIF range instead of the stress range, it follows that:

$$\Delta K_{\mathrm{rms}} = 0.459\Delta K_{\mathrm{max}} \tag{53}$$

By substituting the previous equation into Eq. (51) it results in that:

$$E\left[\frac{da}{dn}\right]_{\mathrm{VA}} = C(0.459\Delta K_{\mathrm{max}})^{m} \tag{54}$$

Therefore, for the truncated Rayleigh spectrum used in [65,66,83], C_{Ω} is related to C by the following relationship

$$C_{\Omega} = 0.459^{m}\, C \tag{55}$$

The predicted fatigue life obtained using the proposed model, is compared to the prediction obtained using the models in BS7910, and the VA fatigue crack growth data. The models in BS7910 are again the "simplified law" or "bilinear law" with the same threshold condition as defined for CA loading. The fatigue crack growth rate for VA loading is estimated as the average of the fatigue crack growth rate $(da/dn)_i$ estimated for each individual stress range of the spectrum, $(da/dn)_i$, weighted by the relative frequency, $n_i/(\sum n_i)$ associated with each stress range of the spectrum, $\Delta\sigma_i$:

$$\left(\frac{da}{dn}\right)_{\mathrm{VA}} = \sum_i \left[\left(\frac{da}{dn}\right)_i \frac{n_i}{\sum n_i}\right] \tag{56}$$

where $(da/dn)_i$ is individually estimated for each stress range of the spectrum by either using the bilinear or the simplified law.

The resulting predicted fatigue life and the comparison with test data are shown in Fig. 15 by either considering residual stresses (using Eq. (30)) or neglecting their effect. This distinction is made because it is likely that the approach in BS7910 might lead to conservative prediction. The predicted curves reasonably bound the average fatigue life following from the VA fatigue test data, depending on the assumed magnitude of the secondary stresses. In particular, the prediction obtained by assuming $\sigma_{\mathrm{r}} = 0$ is inside the 95% confidence interval for the mean response of the LRM fitting the VA fatigue test data. When compared to the fatigue life predicted using the proposed model, the prediction obtained by the models in BS7910 gives conservative results, also with respect to VA fatigue test data.

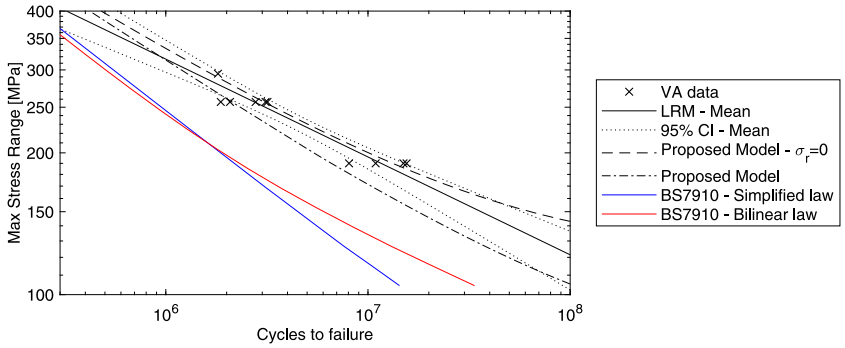

Fig. 15. Comparison between VA fatigue test data from [83], and fitted using a LRM, the 95% confidence interval for the mean response, the prediction using the proposed model with and without residual stresses, and prediction using the models in BS7910.

5. Conclusions

The paper presents a fatigue life prediction model for transverse welded details by making use of the linear elastic fracture mechanics parameter ΔK, considering the behavior of mechanically short (small) and long cracks.

The transition in the threshold condition between small and long cracks is modeled using the exponential relation introduced by McEvily [56]. The parameters of controlling the length scales at which extrinsic phenomena become fully active are estimated by making use of the empirical correlations proposed by Chapetti [46] and Murakami [54]. The comparison between the predicted cyclic R-curve and the test data from literature reveals that the proposed approach determines a non-biased prediction of the threshold condition for small and long cracks. Moreover, following the comparison between the predicted cyclic R-curve and the test data, the global uncertainty has been evaluated based on the distribution of the log-residuals of the threshold stress intensity factor range: CoV=0.10. This performance is better than for other models from the literature. The authors consider the proposed approach as preferable, because of three reasons: (1) it appears to be less biased, (2) leads to a less scattered distribution of the log-residuals, and (3) it requires fewer input variables. In particular, it requires only the Vickers hardness, which can be easily measured, and the threshold of the SIF range for long cracks, which can be measured relatively easily, e.g. in comparison to $\Delta K_{\mathrm{th,eff}}$, and is reasonably known for many steel grades.

Since the correlations developed by Murakami [54,55] are used to estimate relevant quantities such as the intrinsic threshold of the SIF range and the distance from the free surface of the first microstructural barrier, the test data used by Murakami [54] are re-analyzed using the maximum likelihood method in order to estimate aleatory and epistemic uncertainty.

With the aim of predicting the fatigue life at relatively high stress ranges and the fatigue limit of the considered welded detail, it results that the most relevant parameters are the intrinsic threshold of the SIF range and the fatigue crack growth rate coefficient.

The obtained prediction is compared with independent datasets from literature related to a non-load carrying cruciform joint. A good agreement is obtained for both the CA and the VA fatigue life prediction, and a less conservative prediction is obtained as compared to the models in BS7910. The VA fatigue test data were obtained by applying a random block of VA loading by sampling from a Rayleigh spectrum. It is well known that the fatigue strength is strongly related to the type of applied load history. This implies that the estimators of the model parameters derived in this paper cannot be directly applied to predict the fatigue life in the case of a different type of stress spectrum. This would require that either the fatigue crack growth rate be experimentally determined for the selected type of load history (stress spectrum), or crack growth retardation and acceleration models be available and sufficiently accurate to estimate the fatigue crack growth rate for the selected type of load history.

The modification of the residual stress state induced by the VA loading has been considered by two extreme cases: (1) by using the approach for proof loading described in the BS7910, leading to a conservative prediction, and (2) by neglecting the effect of residual stresses, leading to an optimistic prediction. The two predictions are found to reasonably bound the average fatigue life.

Declaration of competing interest

The authors declare that they have no known competing financial interests or personal relationships that could have appeared to influence the work reported in this paper.

Acknowledgments

The authors would like to thank the Dutch infrastructural asset owners ProRail and Rijkswaterstaat and the research organization TNO for their support. Moreover, they are grateful to Prof.dr. Alain Nussbaumer and Prof.dr.ir. Mirek Kaminski for their reflections and contributions to this work.

References

[1] EN 1993-1-9. Eurocode 3: Design of steel structures - part 1-9: Fatigue. Brussels: CEN; 2005.
[2] Sonsino CM. Principles of variable amplitude fatigue design and testing. In: McKeighan P, Ranganathan N, editors. Fatigue testing and analysis under variable amplitude loading conditions. West Conshohocken, PA: ASTM International; 2005, p. 3–23.
[3] Zhang Y-H, Maddox S. Investigation of fatigue damage to welded joints under variable amplitude loading spectra. Int J Fatigue 2009;31(1):138–52.
[4] Kachanov LM. Introduction to continuum damage mechanics. Martinus Nijhoff Publishers; 1986.
[5] Zerbst U, Ainsworth R, Beier HT, Pisarski H, Zhang Z, Nikbin K, Nitschke-Pagel T, Münstermann S, Kucharczyk P, Klingbeil D. Review on fracture and crack propagation in weldments–a fracture mechanics perspective. Eng Fract Mech 2014;132:200–76.
[6] Zerbst U, Madia M, Schork B. Fracture mechanics based determination of the fatigue strength of weldments. Procedia Struct Integr 2016;1:10–7.
[7] Zerbst U, Madia M, Vormwald M. Fatigue strength and fracture mechanics. Procedia Struct Integr 2017;5:745–52.
[8] Zerbst U. Application of fracture mechanics to welds with crack origin at the weld toe: a review part 1: Consequences of inhomogeneous microstructure for materials testing and failure assessment. Weld World 2019;63(6):1715–32.
[9] Zerbst U. Application of fracture mechanics to welds with crack origin at the weld toe—a review. Part 2: welding residual stresses. Residual and total life assessment. Weld World 2019;1–19.
[10] Zerbst U, Vormwald M, Pippan R, Gänser H-P, Sarrazin-Baudoux C, Madia M. About the fatigue crack propagation threshold of metals as a design criterion–a review. Eng Fract Mech 2016;153:190–243.
[11] Chapetti MD. A simple model to predict the very high cycle fatigue resistance of steels. Int J Fatigue 2011;33(7):833–41.
[12] Chapetti MD, Jaureguizahar LF. Fatigue behavior prediction of welded joints by using an integrated fracture mechanics approach. Int J Fatigue 2012;43:43–53.
[13] Chapetti MD, Steimbreger C. A simple fracture mechanics estimation of the fatigue endurance of welded joints. Int J Fatigue 2019;125:23–34.
[14] Maljaars J, Vrouwenvelder T. Fatigue failure analysis of stay cables with initial defects: Ewijk bridge case study. Struct Saf 2014;51:47–56.
[15] Maljaars J, Vrouwenvelder A. Probabilistic fatigue life updating accounting for inspections of multiple critical locations. Int J Fatigue 2014;68:24–37.
[16] Maljaars J, Steenbergen H, Vrouwenvelder A. Probabilistic model for fatigue crack growth and fracture of welded joints in civil engineering structures. Int J Fatigue 2012;38:108–17.
[17] Zhao Z, Haldar A. Bridge fatigue damage evaluation and updating using non-destructive inspections. Eng Fract Mech 1996;53(5):775–88.
[18] Righiniotis TD, Chryssanthopoulos MK. Fatigue and fracture simulation of welded bridge details through a bi-linear crack growth law. Struct Saf 2004;26(2):141–58.
[19] Suresh S. Fatigue of materials. Cambridge university press; 1998.
[20] Carpinteri A, Brighenti R. Part-through cracks in round bars under cyclic combined axial and bending loading. Int J Fatigue 1996;18(1):33–9.
[21] Carpinteri A, Vantadori S. Sickle-shaped surface crack in a notched round bar under cyclic tension and bending. Fatigue Fract Eng Mater Struct 2009;32(3):223–32.
[22] Pucillo GP, Esposito L, Leonetti D. On the effects of unilateral boundary conditions on the crack growth rate under cycling bending loads. Int J Fatigue 2019;124:245–52.
[23] Pearson S. Initiation of fatigue cracks in commercial aluminium alloys and the subsequent propagation of very short cracks. Eng Fract Mech 1975;7(2):235–47.
[24] Otegui J, Burns D, Kerr H, Mohaupt U. Growth and coalescence of fatigue cracks at weld toes in steel. Int J Press Vessel Pip 1991;48(2):129–65.
[25] Otegui J, Mohaupt U, Burns D. Effect of weld process on early growth of fatigue cracks in steel t joints. Int J Fatigue 1991;13(1):45–58.
[26] Otegui J, Kerr H, Burns D, Mohaupt U. Fatigue crack initiation from defects at weld toes in steel. Int J Press Vessel Pip 1989;38(5):385–417.
[27] Mikkola E, Murakami Y, Marquis G. Fatigue life assessment of welded joints by the equivalent crack length method. Procedia Mater Sci 2014;3:1822–7.
[28] Liu Y, Mahadevan S. Probabilistic fatigue life prediction using an equivalent initial flaw size distribution. Int J Fatigue 2009;31(3):476–87.
[29] Zerbst U, Madia M. Fracture mechanics based assessment of the fatigue strength: approach for the determination of the initial crack size. Fatigue Fract Eng Mater Struct 2015;38(9):1066–75.
[30] Zerbst U, Madia M, Vormwald M, Beier HT. Fatigue strength and fracture mechanics–a general perspective. Eng Fract Mech 2018;198:2–23.
[31] Schork B, Kucharczyk P, Madia M, Zerbst U, Hensel J, Bernhard J, Tchuindjang D, Kaffenberger M, Oechsner M. The effect of the local and global weld geometry as well as material defects on crack initiation and fatigue strength. Eng Fract Mech 2018;198:103–22.
[32] Schijve J. Fatigue of structures and materials. Springer Science & Business Media; 2001.
[33] Madia M, Zerbst U, Th. Beier H, Schork B. The ibess model – elements, realisation and validation. Eng Fract Mech 2018;198:171–208. http://dx.doi.org/10.1016/j.engfracmech.2017.08.033, URL http://www.sciencedirect.com/science/article/pii/S0013794417304885 Fracture mechanics-based determination of the fatigue strength of weldments.
[34] Hudak Jr S, McClung R, Bartlett M, Fitzgerald J, Russell D. A Comparison of Single-Cycle Versus Multiple-Cycle Proof Testing Strategies. (Interim report, Nov. 1987- Aug. 1989), 1990.
[35] James M, Smith G. Crack closure and surface microcrack thresholds. Some experimental observations. Int J Fatigue 1983;5(2):75–8.
[36] Ritchie R. Near-threshold fatigue-crack propagation in steels. Int Met Rev 1979;24(1):205–30.
[37] Suresh S, Ritchie R. Propagation of short fatigue cracks. Int Met Rev 1984;29(1):445–75.
[38] Lawson L, Chen E, Meshii M. Near-threshold fatigue: a review. Int J Fatigue 1999;21:S15–34.
[39] Pippan R, Berger M, Stüwe H. The influence of crack length on fatigue crack growth in deep sharp notches. Metall Trans A 1987;18(3):429–35.
[40] Miller K. The two thresholds of fatigue behaviour. Fatigue Fract Eng Mater Struct 1993;16(9):931–9.
[41] Maierhofer J, Pippan R, Gänser H-P. Modified NASGRO equation for physically short cracks. Int J Fatigue 2014;59:200–7.
[42] Ritchie RO. The conflicts between strength and toughness. Nat Mater 2011;10(11):817–22.
[43] Kitagawa H. Applicability of fracture mechanics to very small cracks or the cracks in the early stage. In *Proc. of 2nd ICM*, Cleveland, 1976, p. 627–31.
[44] Suresh S, Ritchie R. On the influence of environment on the load ratio dependence of fatigue thresholds in pressure vessel steel. Eng Fract Mech 1983;18(4):785–800.
[45] Boyce B, Ritchie R. Effect of load ratio and maximum stress intensity on the fatigue threshold in ti–6al–4v. Eng Fract Mech 2001;68(2):129–47.
[46] Chapetti MD. Fatigue propagation threshold of short cracks under constant amplitude loading. Int J Fatigue 2003;25(12):1319–26.
[47] Li B, Rosa L. Prediction models of intrinsic fatigue threshold in metal alloys examined by experimental data. Int J Fatigue 2016;82:616–23.
[48] Liaw PK, Lea T, Logsdon W. Near-threshold fatigue crack growth behavior in metals. Acta Metall 1983;31(10):1581–7.
[49] Wasén J, Heier E. Fatigue crack growth thresholds—the influence of Young's modulus and fracture surface roughness. Int J Fatigue 1998;20(10):737–42.
[50] Tanaka K, Akiniwa Y. Resistance-curve method for predicting propagation threshold of short fatigue cracks at notches. Eng Fract Mech 1988;30(6):863–76.
[51] Smith R. On the short crack limitations of fracture mechanics. Int J Fract 1977;13(5):717–20.
[52] El Haddad M, Topper T, Smith K. Prediction of non propagating cracks. Eng Fract Mech 1979;11(3):573–84.
[53] Kocak M, Webster S, Janosch J, Ainsworth R, Koers R. FITNET fitness-for-service PROCEDURE - section 7: Fatigue module. Tech.rep., European Fitness for Service Network; 2006.
[54] Murakami Y, Endo M. Effects of defects, inclusions and inhomogeneities on fatigue strength. Int J Fatigue 1994;16(3):163–82.
[55] Murakami Y, Beretta S. Small defects and inhomogeneities in fatigue strength: experiments, models and statistical implications. Extremes 1999;2(2):123–47.

[56] McEvily A, Endo M, Murakami Y. On the relationship and the short fatigue crack threshold. Fatigue Fract Eng Mater Struct 2003;26(3):269–78.
[57] Maierhofer J, Kolitsch S, Pippan R, Gänser H-P, Madia M, Zerbst U. The cyclic R-curve–determination, problems, limitations and application. Eng Fract Mech 2018;198:45–64.
[58] Patankar R, Ray A, Lakhtakia A. A state-space model of fatigue crack growth. Int J Fract 1998;90(3):235–49.
[59] Hudson J, Chang C. STP748 - Methods and models for predicting fatigue crack growth under random loading. West Conshohocken, PA: ASTM International; 1981.
[60] Richard HA, Sander M. Fatigue crack growth. Springer; 2016.
[61] Matsuoka S, Tanaka K. Delayed retardation phenomenon of fatigue crack growth resulting from a single application of overload. Eng Fract Mech 1978;10(3):515–25.
[62] Matsuoka S, Tanaka K. The influence of sheet thickness on delayed retardation phenomena in fatigue crack growth in ht80 steel and a5083 aluminium alloy. Eng Fract Mech 1980;13(2):293–306.
[63] Wang G, Blom AF. A strip model for fatigue crack growth predictions under general load conditions. Eng Fract Mech 1991;40(3):507–33.
[64] Borrego L, Ferreira J, Da Cruz J, Costa J. Evaluation of overload effects on fatigue crack growth and closure. Eng Fract Mech 2003;70(11):1379–97.
[65] Barsom J. Fatigue-crack growth under variable-amplitude loading in ASTM A514-b steel. In: Progress in flaw growth and fracture toughness testing. West Conshohocken, PA: ASTM International; 1973.
[66] Fisher JW, Mertz DR, Zhong A. Steel bridge members under variable amplitude long life fatigue loading - National Cooperative Highway Research Program Report 267. Transportation Research Board, National Research Council; 1983.
[67] Guide on methods for assessing the acceptability of flaws in metallic structures. Standard, BS 7910:2013 + A1:2015, BSI Standard Publication; 2012.
[68] Tada H, Paris P, Irwin G. The analysis of cracks handbook, Vol. 2. New York: ASME Press; 2000, p. 1.
[69] Fett T, Munz D, Neumann J. Local stress intensity factors for surface cracks in plates under power-shaped stress distributions. Eng Fract Mech 1990;36(4):647–51.
[70] Fett T. Stress intensity factors-t-stresses-weight functions. Karlsruhe: KIT Scientific Publishing; 2008.
[71] Leonetti D, Maljaars J, Snijder HH. Fitting fatigue test data with a novel sn curve using frequentist and bayesian inference. Int J Fatigue 2017;105:128–43.
[72] Newman JC. A finite-element analysis of fatigue crack closure. In: Rice J, Paris P, editors. Mechanics of crack growth. West Conshohocken, PA: ASTM International; 1976, p. 281–301.
[73] Walbridge S. A probabilistic study of fatigue in post-weld treated tubular bridge structures. Tech. rep., EPFL; 2005.
[74] McClung R. A literature survey on the stability and significance of residual stresses during fatigue. Fatigue Fract Eng Mater Struct 2007;30(3):173–205.
[75] Miller A. Review of limit loads of structures containing defects. Int J Press Vessel Pip 1988;32(1–4):197–327.
[76] Kawagoishi N, Chen Q, Nisitani H. Significance of the small crack growth law and its practical application. Metall Mater Trans A 2000;31(8):2005–13.
[77] Lukas P, Kunz L, Weiss B, Stickler R. Notch size effect in fatigue. Fatigue Fract Eng Mater Struct 1989;12(3):175–86.
[78] Tanaka K, Nakai Y, Yamashita M. Fatigue growth threshold of small cracks. Int J Fract 1981;17(5):519–33.
[79] Shapiro SS, Wilk MB. An analysis of variance test for normality (complete samples). Biometrika 1965;52(3/4):591–611.
[80] Pawitan Y. In all likelihood: statistical modelling and inference using likelihood. Oxford University Press; 2001.
[81] Mischke CR. Prediction of stochastic endurance strength. J Vib Acoust Stress Reliab Des 1987;109(1):113–22.
[82] Klippstein KH, Schilling CG. Stress spectrums for short-span steel bridges. In: Fatigue crack growth under spectrum loads. ASTM International; 1976.
[83] Klippstein KH, Schilling CG. Pilot study on the constant and variable amplitude behavior of transverse stiffener welds. J Construct Steel Res 1989;12(3–4):229–52.
[84] King R. UK: Health and Safety Executive Norwich; 1998.
[85] JCSS. Probabilistic model code. Joint Comm Struct Saf 2001.
[86] Agostoni N, Ballio G, Poggi C. Statistical analysis of the mechanical properties of structural steel. Costr Metalliche 1994;2(XLVI):31–9.
[87] de Jesus AMP, Matos R, Fontoura BF, Rebelo C, da Silva LS, Veljkovic M. A comparison of the fatigue behavior between S355 and S690 steel grades. J Constr Steel Res 2012;79:140–50.
[88] Det Norske Veritas. Oslo, Norway: Det Norske Veritas & Germanischer Lloyd SE; 2015.
[89] Det Norske Veritas. Fatigue strength analysis for mobile offshore units. Classification Note No. 30.2, 1984.
[90] Snijder H, Gijsbers F, Dijkstra O, Avest F. Probabilistic fracture mechanics approach of fatigue and brittle fracture in tubular joints. Elsevier Science Publishers; 1987, p. 927–39.
[91] Maddox S. An analysis of fatigue cracks in fillet welded joints. Int J Fract 1975;11(2):221–43.